The influence of resolution in simulating inter-annual and inter-decadal variability in a coupled ocean-atmosphere GCM, with emphasis over the North Atlantic.

C.Laurent, H.Le Treut, Z.X.Li, L.Fairhead and J.L.Dufresne.

Laboratoire de Météorologie Dynamique du CNRS
Université Pierre et Marie Curie
4, place Jussieu 75252 Paris cedex05.

Abstract

Multidecadal numerical experiments have been realized at different resolutions using the coupled ocean-atmosphere general circulation model developed at IPSL (Institut Pierre Simon Laplace) in Paris. The atmospheric LMD model and the oceanic OPA-LODYC model are coupled without any flux adjustment. The mean simulated climate is stable and differs from reality through a few well established systematic errors. The variability simulated by the model at these different resolutions is compared for various areas, and more specifically the North Atlantic. A statistical method, the Multi-channel Singular Spectrum Analysis (M-SSA), is used to detect sea surface temperature oscillations at different time scales. Oscillations over the North Atlantic display a well-known tripole feature, which seems to depend primarily on the ocean resolution. The period of the oscillation (from 8 to 12 years) seems more sensitive to the atmospheric resolution.

1 Introduction

Understanding the mechanisms of low frequency climate variability at inter-annual or inter-decadal time scale is the key to any kind of prediction. Low-frequency variability can be periodic, quasi-periodic or chaotic and distinguishing those behaviours is essential.
Many authors have studied climate variability based on observations in different areas of the globe, especially in the North Atlantic where deep waters form and where surface temperature anomaly variations at decadal time scales have been observed. Bjerknes (1964) found that low-frequency sea surface temperature changes in the North Atlantic are linked to the variations of the thermohaline circulation. More recently, Hansen and Bezdek (1996) described the spatial and temporal evolution of sea surface temperature anomalies (data from COADS, Comprehensive Ocean Atmosphere Data Set) during 45 years in the North Atlantic and found periods from 3 to 10 years. Sutton and Allen (1997) explained decadal sea surface temperature fluctuations in the North Atlantic with an advective mechanism and suggested this to be part of a coupled ocean-atmosphere mode. Hurrell and Van Loon (1997) showed that decadal climate variations are associated to the North Atlantic Oscillation (NAO).
Oceanic and Atmospheric GCMs (OGCMs and AGCMs) have also constituted useful tools to study climate variability. For example, Weaver and Sarachik (1991) used an OGCM with a constant forcing to study decadal oscillations in the South Atlantic. Graham et al. (1994) used an AGCM to study the response of inter-annual and inter-decadal atmospheric variability in the Northern Hemisphere to sea surface temperature anomalies placed in different areas of the globe (global, tropical and mid-latitudes anomalies).
During the recent years, it has also become possible to use Coupled ocean-atmosphere GCMs at these time scales. For example, in the North Pacific, Latif and Barnett (1994) found that variations of sea surface temperature and integrated temperature over the first 500 meters of the ocean are following the subtropical gyre motion with a 20-year period. In the North Atlantic, Delworth et al. (1993) explained inter-decadal variations of the thermohaline circulation by an oceanic role (advection by the subpolar gyre).
Models thus confirm the existence of inter-decadal oscillations, and they provide mechanisms. These mechanisms, however, cannot be fully assessed through the rather scarce available data sets. It is therefore extremely important to assess the robustness of the model results, to many features, and particularly to the horizontal grid resolution.

We use the IPSL (Institut Pierre Simon Laplace) model which is constituted by the coupling of the LMD (Laboratoire de Météorologie Dynamique) atmospheric model and the OPA-LODYC (Laboratoire d'Océanographie DYnamique et de Climatologie) oceanic model at different resolutions. We call in the paper "High" atmospheric resolution a resolution of about 3.5 degrees: 96 points regularly spaced in longitude, 72 points regularly spaced in sine of the latitude and 15 vertical layers. We call "Low" atmospheric resolution a resolution of about 5 degrees: 64 points regularly spaced in longitude, 50 points regularly spaced in sine of the latitude and 11 vertical layers. In the same manner, we call "High" oceanic resolution a resolution of about 2 degrees for longitude and 1.5 degrees for latitude at mid-latitudes, and 0.5 degrees at the equator: 182 points in longitude, 152 points in latitude and 31 vertical layers. We call "Low" oceanic resolution a resolution of about 4 degrees in longitude and about 1 degree at the equator to 4 degrees in latitude: 92 points in longitude, 76 points in latitude and 30 vertical layers. The version of the coupled model called afterwards HH couples the "High" resolutions of both the atmosphere and the ocean, the version called LL couples the "Low" resolutions of both the atmosphere and the ocean, and we will refer also to a third version called HL with a "High" resolution ocean and a "Low" resolution atmosphere. HL has a slightly different physics (it includes a refined sea-ice model), is a more recent simulation than the two others and we will use its results less systematically than those of HH and LL. The model climatology is described in details in a companion paper (Fairhead et al. 1998).

The model components and the experimental design are described in Section 2. The mean state of the coupled simulations is also briefly described in the same section. Section 3 presents the simulated sea surface temperature variability, and also briefly, the statistical method used for our study. Then, section 4 concentrates on the sea surface temperature variability in the North Atlantic ocean, with a particular emphasis given to the quasi-decadal sea surface temperature oscillation simulated in the HH simulation. We conclude the paper in Section 5 with a summary and directions for future work.

2 Model description and design of the experiment

The version of the IPSL model corresponding to the HH and LL simulations is called IPSL1, and it has been used for the CMIP1 (Coupled Models Intercomparison Project Phase 1) experiment (the few differences between HH and LL are listed below in section 2.3). The version corresponding to the HL simulation has been defined for the CMIP2 experiment and mainly differs through the treatment of sea-ice and some details of the cloud physics.

2.1 The atmospheric model

The atmospheric model is the LMD AGCM developed at the Laboratoire de Météorologie Dynamique (LMD) and described in Sadourny and Laval (1984) . The version being used is LMD5.3 (cycle 5), described in Harzallah and Sadourny (1995) . The model is a finite difference general circulation model based on a staggered Arakawa C-grid. Grid points are regularly spaced in longitude and in sine of latitude. The grid has equal area meshes, with a better latitudinal resolution in low latitudes. The model uses sigma coordinates as vertical coordinates. Primitive equations are expressed in terms of u and v wind components, potential enthalpy, specific humidity and surface pressure. Time stepping is a combination of Matsuno and leap-frog schemes. The advection scheme is designed to conserve potential enstrophy for divergent barotropic flow (Sadourny 1975a and 1975b). Lateral diffusion is modeled by a mixed bi-Laplacian operator. Short-wave radiation is modeled after an updated version of the scheme of Fouquart and Bonnel (1980) and distinguishes two spectral intervals: visible and near infrared. Long-wave radiation is computed after the method of Morcrette (1990) over 7 spectral intervals for LL. A new release of the Morcrette's scheme has been introduced in HH and HL. The cloud overlapping is then random-maximum instead of being only random in the previous version. Some other minor modifications on clear sky affect slightly the radiative transfer. An iterative method is used in which saturation is tested downward starting from the top layer to allow the falling droplets to evaporate. Kuo's scheme (1964) deals with convection due to large scale moisture convergence.

Manabe and Strickler's (1964) moist convective adjustment occurs when the air is super-saturated (small-scale convection). The Le Treut and Li's (1991) cloud parameterization is based on a cloud water budget equation. The interaction with radiation makes explicit use of the computed cloud fraction and cloud water content but uses prescribed equivalent droplet radius.

2.2 The oceanic model

The oceanic model is the OPA OGCM developed at the Laboratoire d'Océanographie DYnamique et de Climatologie (LODYC) (Delecluse et al., 1993) to study large-scale ocean circulation and its interaction with atmosphere and sea-ice. The version used in the paper is OPA7G onto a global ocean domain. The model solves the primitive equations with a non-linear equation of state (Unesco, 1983). Equations are discretised on a staggered Arakawa C-grid. Time stepping for advection, Coriolis and pressure terms is achieved by a leap-frog scheme associated with an Asselin filter applied at each time step in order to avoid time splitting. A rigid lid approximation is made at the surface. First used for process and basin studies, the code was adapted to the global ocean (Madec and Imbard, 1996). A distinctive feature of the model grid is that, in the southern hemisphere, it is regular, while in the northern hemisphere, the grid is stretched with the pole centered on Asia to overcome the North pole singularity (Madec and Imbard, 1996). The horizontal mesh is orthogonal and curvilinear on the sphere. The bathymetry is derived from ETOP5, a 5 minutes by 5 minutes gridded global bathymetry file provided by the Marine Geology and Geophysics Division/National Geophysical Data Center. The model comprises 11 islands (Antarctica, America, New Zealand, Australia, Madagascar, New Guinea, Borneo, Philippines, Cuba, Iceland and Spitzbergen). The Bering strait is open.

The lateral diffusive and dissipative operators are second order ones. Operators acting on momentum, temperature and salinity are of Laplacian type. In the version used, the diffusion is isopycnal. The horizontal eddy viscosity depends on the geographical position (it is taken as $40000 m^2.s^{-1}$ in the interior and is reduced near the western coats and near the equator to $2000 m^2.s^{-1}$). The vertical eddy viscosity and diffusivities are computed by a 1.5 order Turbulent Kinetic Energy (TKE) closure scheme (Blanke and Delecluse, 1993) which allows the formulation of the mixed layer as well as a minimum diffusion in the thermocline. An implicit scheme is used for vertical diffusive processes. The solar radiation penetrates in the top meters of the ocean (Blanke and Delecluse, 1993). Absorption is indeed very selective in the first ten meters of the ocean. The ocean tends to absorb preferably the longest and the shortest wavelengths. A formulation including extinction coefficients is assumed for the downward irradiance I (Paulson and Simpson, 1977), taking this selective absorption in the ten first meters of the ocean into account. Deeper, irradiance evolves with an exponential decay of the surface irradiance. The values of these extinction coefficients correspond to a Type I water in Jerlov's (1978) classification.

Two of the versions used in the paper (HH and LL) don't include a sea-ice component but a simple test on sea surface temperature. Ice appears when the ocean surface temperature becomes less than the freezing temperature. A constant heat flux is then applied to the ocean under the ice ($-2 W.m^{-2}$ in the Arctic ocean and $-4 W.m^{-2}$ in the southern ocean) to take the insulating effect of ice into account. The AGCM above computes its own surface heat flux (in coupled versions). On the other hand, the intermediate resolution version (HL) has a sea-ice thermodynamic scheme (OPAICE), which is described in Fairhead et al. (1998).

2.3 Design of the experiment

The LMD and OPA models are coupled through the OASIS (Ocean Atmosphere Sea Ice Soil) coupler developed at CERFACS (Centre Européen de Recherche et de Formation Avancée en Calcul Scientifique) in its version 2 (Terray, 1994). There is no flux adjustment in this coupled model. The coupler does the spatial interpolation from one grid to another and ensures the time synchronization between the two GCMs. The coupler interpolates the net surface heat flux, the solar flux, the net water flux and the wind stresses from the atmosphere model grid to the ocean model grid, and the sea surface temperature and the sea-ice cover from the ocean model grid to the atmosphere model grid. The models exchange time-averaged fields once a day. The low resolution run (LL), carried out at the Laboratoire des Sciences du Climat et de l'Environnement (LSCE) lasts 100 years (it has been continued to 150 years at the present moment). Compared to a first version (Braconnot at al. 1997) where the model was drifting away towards a warm state, a few detail changes (a calculation of the separated fluxes on the fractions of sea-ice and free ocean meshes, a different diffusion threshold in the boundary layer, a convective entrainment, a reduction of the droplet size to 10μm and an isopycnal diffusion) have been sufficient to stabilize the model. For the coupler, the interpolation between the two grids is more conservative. The high resolution one (HH), carried out at the Laboratoire de Météorologie Dynamique (Fairhead et al. 1998), lasts 25 years. The initial state for ocean in LL is a 10-year climatology obtained with Hellerman wind stresses and Esbensen-Kushnir fluxes like forcing. For atmosphere, the model starts with a climatology issued of an AMIP (Atmospheric Models Intercomparison Project) run. The initial state for ocean in HH is a restart from Levitus. For the atmosphere, we start with a climatology issued of an AMIP (Atmospheric Models Intercomparison Project) run. The intermediate resolution version (HL) contains a more complex physics (with a different threshold for the transition phase between liquid and ice clouds, and a different law for the overlapping of clouds for examples) and a sea-ice thermodynamical scheme. This HL run starts for the ocean from Levitus observations and from the 1st January 89 of an AMIP run for the atmosphere. Then a period of 8 years is forced towards climatology. From year 9 and after a rapid initial drift the model reaches a quasi-equilibrium at year 15. The coupled simulation itself lasts 100 years. The years 30-98 (therefore a total of 69 years) are studied in the following. This simulation has been continued to 200 years. This HL version will be used for settling on the effect of resolution on climate variability when necessary. The principal characteristics and differences between these three versions are summarized in Table 1.

2.4 Mean state of the coupled simulation

Although these simulations are described in more details elsewhere (Fairhead et al. 1998), it is necessary to give some elements of the mean climate simulated by LL, HH and HL.
The main characteristics common to LL, HH and HL are the following: the simulation stabilizes after a few years in global average. Compared with Reynolds observations, middle and high latitudes (40^oN-70^oN;40^oS-60^oS) are too hot of about 2 to 4^oC (Figures 1 and 2) and are getting hot during the simulation (Figure 4 mainly and Figure 5 for middle and high latitudes of the southern hemisphere). This heat penetrates the first hundreds meters of the ocean near 60^oS mainly (Figure 4). In HL this warming is widely corrected (Figure 5). Sea-ice is melting completely in the Antarctic in both the HH and LL simulations whereas ice is maintained only in winter in the Arctic (not shown). The HL simulation is much improved for that matter as explained below.
On the contrary, in the tropical latitudes (30^oS-30^oN), sea surface temperatures are too cold of at least 2^oC compared with Reynolds observations (Figures 1 and 2). The tropics are less cold in HH than in LL. Warm surface waters of the west tropical Pacific are strongly reduced by the progression of a cold equatorial tongue westward, but the equatorial east-west sea surface temperature gradient is maintained (not shown). In the tropical Pacific of HH for example, at surface, the isotherm 27^oC disappears after the two first years of the run but reappears at the fourteenth year and is maintained (Figure 3). The various coupled models using the LMD GCM all tend to show the westward extension of the cold tongue in the tropical Pacific, independently of the nature of the ocean model, which can be a thermodynamical model (Musat, 1998, personal communication) or a different OGCM (Grenier et

al. 1998 , using the Université Catholique de Louvain OGCM), and independently of the resolution of both the ocean and the atmosphere (as shown for example by the HL model). The tropical troposphere is getting cold during the simulation (Figures 4 and 5).
In HL simulation, the strong heating present in HH near 60^oS and beyond 60^oN is reduced. It shows a relative cooling in the high latitudes of the northern hemisphere even if between 40^oN and 60^oN there is a heating near the surface of the ocean and in the ocean itself (Figure 5). Sea-ice in the Arctic is maintained and stable even if the melting in summer is not strong enough (not shown). During the period when sea surface temperature is forced towards Levitus climatology (first 8 years), the sea-ice extend in the Antarctic is close to the observations. When the coupled model is free (at year 9), it diminishes of about 50% in comparison with the observations. Then, it diminishes again of about 40% after about 40 years of coupled run but tends to reform on and after year 40 (not shown).
In spite of the systematic errors mentioned above, the simulations are stable enough, and close enough from the observations in some key areas such as the North Atlantic, to study usefully the climate fluctuations.

3 Simulated sea surface temperature variability

3.1 General features

To study the simulated climate variability, global monthly fields calculated by the coupled model are used. A first step is to determine the areas of the globe where the model simulates some variability at inter-annual scales. To do so, the standard deviation, or the root-mean square (rms), of sea surface temperature (SST) is calculated. The mean annual cycle is removed from data since we are interested in longer time scales.

Sea Surface Temperatures (SSTs) are a good indicator of both the atmospheric and the oceanic variability. The global standard deviation of sea surface temperature (mean annual cycle removed) is plotted for LL in Figure 6, for HH in Figure 7, and for comparison, for GISST2 observations in Figure 9, from 60^oN to 60^oS to avoid sea-ice areas. These observations of sea surface temperature cover the period 1903-1994 and are distributed on a $1^o * 1^o$ grid. We use these data on an interpolated grid (which is the atmospheric grid of the HH version) for the global study, and we use original data ($1^o * 1^o$) for regional studies. Figures 6 and 7 show areas of the globe where the coupled model simulates inter-annual variability for sea surface temperature. These are mainly the North Atlantic, the North Pacific (Kuroshio current zone) and the circumpolar current area, whatever the resolution. Compared to the observations (Figure 9), HH gives a stronger weight to the variability of the North and Tropical Pacific. In observations, east tropical Pacific stands out from other regions with a strong inter-annual variability. The HH simulation does simulate an inter-annual variability in the east tropical Pacific also but with a too weak amplitude compared with other regions and also compared with models with a higher resolution ocean component (Vintzileos et al., 1997). The intermediate resolution version, with a low resolution atmosphere and a high resolution ocean, reproduces better the Pacific tropical variability (Figure 8). But compared with observations, this tropical variability area is propagating too much to the west and is too confined at the equator. In this intermediate resolution version, North Pacific and North Atlantic variabilities are quite well reproduced compared to GISST2 observations. HH also shows a maximum in the variability off the coasts of Argentina, which is more extended geographically than in the GISST2 observations.
The comparison of the HH (Figure 7) and HL (Figure 8) results to those of LL (Figure 6), especially when there are put in perspective through the reference to observations (Figure 9) provides a first crude evidence of the importance of the ocean model resolution.

3.2 Methodology of the analysis

In the following we will try to focus this rough estimate of the model variability through the use of a more advanced statistical method: the Multichannel version of the Singular Spectrum Analysis (M-SSA) (Vautard et al. 1992 , Plaut and Vautard 1994). This method is a natural extension of the SSA to time series of vectors or maps rather than scalars, such as varying temperature over the globe for example.
We outline here the method for univariate time series and generalize for multivariate ones after (Plaut and Vautard 1994). The SSA allows us to obtain from data a sequence of vectors which can be decomposed into elementary oscillatory structures. The starting point of this method is to embed a time serie of data X_i with $1 \leq i \leq N$ in a vector space of dimension M. The embedding procedure constructs a sequence $\tilde{X}_i$ of M-dimensional vectors from the original time serie X, by using lagged copies of the data X_i. The temporal lag j goes from 0 to M-1:

$$\tilde{X}_i = X_{i+j} = (X_i, X_{i+1}, \ldots, X_{i+M-1}), \quad for\ 1 \leq i \leq N - M + 1$$

We then generate the (M*M) temporal covariance matrix T_X. The eigenelements $(E_j^k, \lambda_k), k = 1, \ldots, M$ of this matrix are computed, $T_X\, E_j^k = \lambda_k\, E_j^k$. The eigenvectors E_j^k are called the Temporal Empirical Orthogonal Functions (T-EOFs) and λ_k are their associated eigenvalues. The eigenvalue λ_k define the percentage of variance associated to the kth PC, by the following relation: $\lambda_k / \sum_{k=1}^{M} \lambda_k$ = %variance(PC$_k$). Projecting the field $\tilde{X}_i$ onto each EOF, the corresponding Temporal Principal Components a_i^k (T-PCs) are obtained:

$$a_i^k = \sum_{j=0}^{M-1} X_{i+j}\, E_j^k, \quad where\ i\ varies\ from\ 1\ to\ N - M + 1$$

When two consecutive EOFs (of order k and k+1), whose PCs are in quadrature, have periodic variability and nearly equal eigenvalues, we can reconstruct a part of the time serie associated with these two EOFs, by combining the associated PCs:

$$R_\kappa(t) = \frac{1}{M_t} \sum_{k \in \kappa} \sum_{j=0}^{M-1} a_{i-j}^k\, E_j^k, \quad where\ i\ varies\ from\ 1\ to\ N$$

where κ is the set of EOFs on which the reconstruction is based and M_t is a normalization factor which is M for the central part of the time serie and has slightly different values near its endpoints (see Ghil and Vautard 1991 , Vautard et al. 1992 for more details).

The use of the (M-)SSA for multivariate time series was proposed theoretically, in the context of non-linear dynamics, by Broomhead and King (1986) and applied to large-scale atmospheric fields by Kimoto et al. (1991) and Plaut and Vautard (1994) . This statistical method, using a large number of lags, identifies dynamically coherent space-time patterns dominating the variability, given a regularly sampled archive of maps. We summarize briefly the method. Our treatment follows mainly Plaut and Vautard (1994) and is also inspired from Moron et al. (1996) .

Whatever the field to study is, the field anomalies are first spatially filtered by a classical Principal Components Analysis (PCA) to reduce the dimension of the field, and a few leading eigenmodes are retained (eigenvalues are plotted in decreasing order and the ones distinguishing are kept). The eigenvectors are called the Spatial Empirical Orthogonal Functions (S-EOFs) and their associated time-dependent projection coefficients the Spatial Principal Components (S-PCs). The leading spatial PCs form the "channels" c to be analyzed by the M-SSA (in our study, results are obtained with three tests c=5, c=7 and c=10). We use those channels as the principal directions on which to decompose the signal. We are to analyze a multichannel time series $X_{l,i}$, with $1 \leq l \leq L$ and $1 \leq i \leq N$, l representing the channel number and i representing time. Each channel is assumed to have a zero temporal mean and X is stationary. Like for the SSA described before, a user-prescribed parameter M is introduced, called the window length, or embedding dimension. The following embedded state vector is generated,

$$(X_{1,i}, X_{1,i+1}, \ldots, X_{1,i+M-1}, X_{2,i}, \ldots, X_{2,i+M-1}, \ldots, X_{L,i}, \ldots, X_{L,i+M-1}), \quad with\ 1 \leq i \leq N - M + 1$$

The eigenvalue problem is now of dimension (L*M). The cross-covariance matrix T_X for the chosen temporal lag M is a block-Toeplitz (L*M)*(L*M) matrix, symmetric and nonnegative, of the form:

$$T_X = \begin{pmatrix} T_{11} \ldots T_{1L} \\ T_{21} \ldots T_{2L} \\ \vdots \ldots\ldots \\ T_{L1} \ldots T_{LL} \end{pmatrix}$$

where each $T_{ll'}$ is the M*M lag covariance matrix between channel l and channel l'. Each element is estimated by using a least-bias covariance formula (see Vautard et al. 1992 , Plaut and Vautard 1994). The eigenvectors $E^k_{l,j}$ $(k = 1, L*M)$ of this matrix are calculated. These (L*M) vectors are distinct and called the Space-Time Empirical Orthogonal Functions (ST-EOFs). They are associated with (L*M) eigenvalues, not necessarily distinct. The temporal coefficients a^k_i, called the Space-Time Principal Components (ST-PCs), associated to these ST-EOFs are computed by projecting the embedded field X onto these principal directions.

$$a^k_i = \sum_{j=0}^{M-1} \sum_{l=1}^{L} X_{l,i+j}\, E^k_{l,j}, \quad where\ i\ varies\ from\ 1\ to\ N - M + 1$$

The double summation accounts for the block matrix structure of T_X.
The fundamental property of the M-SSA (Vautard et al., 1992) lies in the fact that when

(i) two consecutive eigenvalues are nearly equal,

(ii) the two corresponding time sequences described by the EOFs are nearly periodic, with the same period, and in quadrature,

(iii) the associated PCs are in quadrature.

then there is in the series an oscillation whose period is the same as the period of the ST-EOFs themselves and whose spatial pattern is the same as the one of the ST-EOF.
Reconstructed Components (RCs) can be obtained by convoluting the corresponding ST-PCs with ST-EOFs. The type of reconstruction used (see Plaut and Vautard 1994) preserves the phase and the sum of all reconstructed components gives back the original time series. For each oscillating pair, the phase index, which varies between 0 and 2π, describes the life cycle of the oscillation (see Moron et al. 1996 for technical details). One can think of this index as being defined on the unit circle. The RCs with index falling within a given sector of 45^o of the circle are averaged. We then obtain a succession of 8 composite maps forming the oscillation (when not specified we choose to decompose the oscillations on 8 phases).

3.3 Applications to global fields

We now present the results of the M-SSA analysis performed on global monthly sea surface temperatures. We remove a seasonal trend and the mean annual cycle from SST fields. The trend is linear and is calculated in a seasonal way: it is calculated for all January months, all February months ...all December months and then this seasonal trend is removed from data. We obtain what we call "SST anomalies". We use three different sizes of window (M) when applying the statistical method M-SSA: 72 months (6 years), 120 months (10 years) and 168 months (14 years), depending on the length of the studied data. In the tables summarizing the results of the M-SSA (Tables 2 to 5), the percentage of variance of the oscillating pair and the main peak period are presented with a mean plus or minus a standard deviation. These results are issued of three different tests on the number of S-PCs kept (number of channels c) for the analysis: c=5, c=7 and c=10, except for the global study which is done with c=5 only.
We analyze the last 80 years of the 100-year LL simulation, the last 17 years of the 25-year HH simulation and 45 years of GISST2 observations (1950-1994) interpolated on the HH atmospheric grid (96 points in longitude and 72 points in sine of the latitude). The first five S-EOFs (Spatial Empirical Orthogonal Function) of sea surface temperature in LL, HH and GISST2 represent about between 20% and 35% of the total variance. A large part of the signal must be retained by the annual cycle. The results obtained with the M-SSA analysis for global ocean are summarized in Table 2 both for the simulations and for the observations. The main oscillating pairs found are associated with spectral peaks near 100 months (about 8 years, or its harmonic) and 40 months (about 3 years). The quasi-decadal oscillation is quite stationary (not shown). Figure 10 shows the root mean square of sea surface temperature for ST-RCs 6-7 in LL (with 5 channels c retained and a window length w of 120 months). The percentage of variance of the pair 6-7 is weak (about 4%), but at the frequency peak it is strongly increased (46%). Figure 11 is the same but for RCs 1-2 (with 5 channels c and a window length w of 72 months) in GISST observations (1950-1994). In this case, the M-SSA is only used as a filter. The Kuroshio current variability of LL dominates the tropical Pacific variability. In the observations, the tropical Pacific variability is dominant. The quasi-decadal oscillation found in HH shows, like L,L extratropical variability, mainly in the North Pacific and in the Antarctic countercurrent area (not shown).

The model, in all its versions, shows some important extratropical variability, which dominates the tropical oscillations. In section 3.4 we analyze briefly this tropical behaviour of the model, because it may affect the extratropical variability, on which we focus our analysis afterwards.

3.4 Tropical Pacific

Sea surface temperature anomalies in the tropical Pacific (defined as the area between 20^oN-20^oS;120^oE-90^oW) are considered for the HH and LL runs and for GISST2 observations. A linear seasonal trend and the mean annual cycle have been removed from data as previously. Results obtained with the M-SSA are summarized in Table 3 for the model and for GISST2 observations. The last 80 years of the 100-year in LL are analyzed. Similarly, the last 17 years of the 25-year of HH and 92 years (1903-1994) of GISST2 observations (on the original $1^o * 1^o$ grid) are also analyzed.
LL and HH simulations show some El-Niño-like oscillations, with sea surface temperature anomalies located at the east Pacific propagating to the west along the equator. The oscillating pairs represent between 13% and 20% of the total variance (see Figures 12 and 13). The two spatial structures of the simulated El-Niño-like oscillation look similar whatever the model resolution, with sea surface temperature anomalies propagating too much to the west of the Pacific, compared to GISST2 observations (Figure 14). Furthermore, the simulated signal is too confined at the equator compared to

observations. In HH, the signal is at least in some areas more confined at the equator than in LL, where in phase 6 of Figure 12 for example, it spreads to the south of the region. Finally, we can detect an El-Niño-like oscillation in HL (analyzed from year 30 to year 98) also (Figure 15). The maximum amplitude of sea surface temperature anomalies (about 0.25^{o}C in phase 8) is closer to the observations than in LL or HH. The spatial structure of this oscillation looks like the one in HH, with a pronounced westward extension of the anomalies at the equator. In the tropical Pacific coupled model, which is constituted of a low resolution atmosphere but a high resolution ocean in the tropical Pacific (see Vintzileos et al 1997), the El-Niño oscillation is also propagating too much west and the signal seems also to be confined at the equator. The amplitude of the signal is of the same magnitude than for HH and HL. Robertson et al. (1995) detect in two 11-year simulations of the UCLA global atmospheric GCM coupled to the GFDL oceanic GCM, using the M-SSA, a weaker simulated inter-annual sea surface temperature variability than observed. The westward propagation is slight in their case.

The coupled model simulates a tropical Pacific sea surface temperature variability, whatever the resolution, even if the amplitude is weaker than in GISST2 observations. This simulated El-Niño-like signal propagates also too much to the west Pacific and is too confined at the equator compared to observations.

3.5 North Pacific

Another important area where there occurs a strong inter-annual signal which may influence the Atlantic is the Pacific. We focus here on sea surface temperatures in winter (mean over December, January and February, DJF), season which allows to take into account signals coming from the ocean interior, because the oceanic mixed layer is deep and well mixed.
We consider the North Pacific region (defined as the area between 0^{o}N-70^{o}N and 120^{o}E-90^{o}W) with 79 years of winter sea surface temperature for LL, 16 winters for HH and 89 winters for GISST2 observations (1904-1992) on the original $1^o * 1^o$ grid. Results obtained with the M-SSA are summarized in Table 4, for the two versions of the model and for the observations. In the North Pacific, we have chosen to display only some geographical indication of where variability occurs. For this purpose, we calculate the correlation coefficient between the temporal coefficient of the first Empirical Orthogonal Function (PC1) of sea surface temperature in this area and the initial field itself. Spatial structures obtained for LL, HH, GISST2 observations and HL are drawn in Figure 16. Percentages of variance are comparable, with values around 20%. We can note that the spatial structures obtained in HH and HL are very similar, even if the high resolution structure is noisier. This similarity may indicate that this sea surface temperature signature is rather oceanic than atmospheric. This structure seems to be shifted to the north-east compared to observations. The LL structure is on the contrary quite different.

The high resolution, at least for the ocean, seems to be important to obtain a correct spatial structure of variability.

4 North Atlantic decadal time-scale oscillation

In the North Atlantic area, GISST2 reconstructions (resolution $1^o * 1^o$) over the period from 1904 to 1992 reveal a decadal oscillation. We analyze here a region from 15^{o}N to 70^{o}N and 75^{o}W to 20^{o}E, to study in more details the existence and characteristics of any similar oscillation in the model. We concentrate on winter season like for the North Pacific region and for the same reason.

4.1 decadal sea surface temperature oscillation

Table 5 summarizes the results obtained using the M-SSA over the North Atlantic sea surface temperature for LL (79 winters), HH (16 winters) and GISST2 observations (89 winters) on the original $1^o{*}1^o$ grid. The percentage of variance represented by the 10 channels kept is higher compared to the one of the only first 5.

The both versions LL and HH of the model simulate a quasi-decadal oscillation. In LL, the spatial structure associated to the detected quasi-decadal sea surface temperature oscillation is rather stationary (Figures 17 and 18), with only a weak propagation of the signal. We find in Phase 1 (respectively Phase 5) a pattern with three extrema, which begin to propagate. But the pattern is then little changed from Phase 2 (respectively Phase 6) to Phase 4 (respectively Phase 8). Only the amplitude changes. The percentage of variance of this oscillating pair (7-8) is weak (5%) but at the peak frequency (about 10 years), it is strongly increased (48%). In HH, the quasi-decadal oscillation detected (Figure 19) represents about 36% of the total variance. The half-cycle (Phases 1 to 4) of this oscillation can be described in this way : positive (negative) anomalies of SST near Newfoundland are propagating towards the south-west following the subtropical gyre movement, while negative (positive) anomalies go from south of Newfoundland to the west of Europe. Different choices of window size have been tested in HH (8 years, 9 years, 10 years and 11 years) to test whether the structure of this oscillation was robust (not shown). The period of the oscillation found can vary a little, but the same spatial structure is found in all cases for SST anomalies (not shown). This quasi-decadal SST oscillation therefore seems to follow a robust spatial organization. We have also tested the LL oscillation by analyzing LL over the same period than HH (over 16 winters). In this case, the quasi-decadal oscillation is also detected (w=10 years, c=5, RCs 1-2, 46% at the frequency peak). In the observations, the spatial structure of the quasi-decadal oscillation (Figures 21 and 22) is somewhat different than in the simulations. The propagating movement, present in the HH oscillation and almost absent in LL, is weak in the observations. The oscillation pattern detected in HH is however closer to the observations than the LL oscillation.

In the North Atlantic HL SSTs (69 winters), a quasi-decadal oscillation is also detected, with a spatial structure closer to the one detected in HH and in the observations than in LL (Figures 23 and 24). The cycle is also quasi-stationary. It therefore seems that a more realistic spatial pattern of the signal is obtained with a higher resolution ocean. This result shows again the importance of the oceanic resolution in simulating inter-decadal extratopical SST variability.

Furthermore, this spatial structure of the quasi-decadal sea surface temperature oscillation in the North Atlantic appears only when analyzing winter anomalies (DJF). The ocean seems to keep memory of this signature from a winter to another. Indeed for summer (JJA), no SST oscillation with similar spatial structure is found, neither in the model nor in the observations (not shown).

4.2 relation between sea surface temperatures and atmospheric surface fields

We now focus on the quasi-decadal sea surface temperature (SST) oscillation detected in the North Atlantic ocean, simulated in HH. This section is of course very qualitative in view of the shortness of our experiments. Its interpretation has very little background but is supplied: (i) by the similarity of the spatial pattern with observations (ii) the physical consistency of the results (iii) the results of the HL simulation, less precise but much longer.

We can mention first that the first two Empirical Orthogonal Functions (EOFs) of sea-level pressure (SLP) simulated by the model in the North Atlantic are the North Atlantic Oscillation (NAO) as first EOF and the Eastern Atlantic mode (EA) as second EOF, as defined in Cayan (1992) . These two simulated modes are quite close to the observations (Cayan, 1992), both from the point of view of spatial structures and in point of view of percentages of variance. HH and HL tend to shift the structures a little too east compared with the observations, and LL tends to shift them to the west (not shown). Again, a higher resolution ocean is associated with a weaker bias. In fact, we can note that the inter-annual and inter-decadal variability in the North Atlantic concerning the sea surface temperature seems to be shifted in LL compared to HH in agreement with the seasonal variability of the sea level pressure in this area (not shown).

We consider Phase 6 of the SST oscillation found in HH. It shows a tripole (see Figure 20), which has been shown by many analysis from data and models (see Kushnir 1994 and Zorita et al. 1992 for observations and Selten et al. 1997 for models for examples). In spite of the brevity of our simulation, we will use it to discuss qualitatively the mechanisms which are responsible for the oscillation. We average the winter northern hemisphere sea-level pressure on the various phases of this oscillation (we take the mean over common dates). In the North Atlantic, for Phase 6 of the 8-year SST oscillation of HH, the results are shown in Figure 25. This SST and SLP pattern looks like the patterns of inter-annual variability in the Atlantic ocean-atmosphere interaction presented by Bjerknes (1964) , and more recently by Kushnir (1994) . In comparison with the analysis of observations from Kushnir (1994) (Figure 11) , the center of action situated off western Europe is quite well located, a little too much to the south-west, but with a correct amplitude. North of about 50^{o}N, negative SST anomalies are associated to a strengthening of the westerly winds (see below). This structure corresponds to a positive phase of the North Atlantic Oscillation (NAO) index, defined as the SLP difference between Açores and Iceland. The North Atlantic Oscillation is the predominant mode of atmospheric variability in the North Atlantic area.

For comparison, the correlation coefficient between winter GISST2 observations ($1^o * 1^o$) and winter NAO index (1903-1992) is calculated and drawn in Figure 26. This NAO index is defined as the normalized sea level pressure differences between Portugal and Iceland (Hurrell and Van Loon 1997). A bilateral Student test at 5% level, testing the following hypotheses on the true correlation (ρ), $H_0 : \rho = 0$ and $H_1 : \rho \neq 0$ with a probability $p = 0.05$, is made to know the significant level for the calculated correlations. This significant level varies with the number of independent observations (90 years here). Correlations greater than 0.2 are statistically significant, with only 5% of chance to have refused H_0 while H_0 is true. We can note that this inter-annual pattern looks like the inter-decadal pattern obtained in Figure 25. This means that, associated with a positive NAO index, with anomalously high SLP over Açores and anomalously low SLP over Iceland, we obtain a zonal SST pattern forming a tripole which looks like Phase 6 of the inter-decadal SST cycle. The behaviour of the atmosphere (visible in the SLP evolution) isn't symmetric during the HH SST cycle.

There is no identical phase with such a SST tripole in the quasi-decadal oscillation of LL, so the atmospheric behaviour is not comparable. In HL, in which Phase 6 shows also this SST tripole, SLP anomalies are also located like a positive NAO index (not shown). In this latter case, the SLP dipole is shifted to the east compared to the HH SLP dipole: the maximum of SLP anomalies is located above Spain. The spatial pattern of SLP in HL associated to the SST tripole is closest to the definition of the NAO index than in HH. Again the higher oceanic resolution gives more realistic results, in terms of spatial structure of the anomalies.

A composite map with the wind stress is also constructed, superposed to the same phase of the HH SST oscillation (Figure 27). The global motion of the wind stress associated to this particular phase of SST is circular, following the subtropical gyre motion. In the north part of this region, the subpolar gyre movement is also visible and westerlies are amplified. So warmer (colder) than normal SSTs coincide with weaker (stronger) than normal westerly winds.

Concerning the surface latent heat flux in winter, the figure 28 shows the meshes of the grid where sea surface temperature and latent heat flux anomalies are of opposite signs, for Phase 6 of the 8-year SST cycle in HH. For most of the region, SST anomalies and latent heat flux anomalies are of opposite signs during this phase. This result may indicate that ocean-atmosphere feedbacks, acting through changes in the turbulent fluxes, play an active role in maintaining sea surface temperature anomalies. This is also true for the sensible heat flux (not shown).

The analysis carried out in this section reveals a consistent physical behaviour of the model in terms of propagation of the SST anomalies at the decadal time-scale, especially in the HH version, in spite of its short length. These anomalies can be simulated in a realistic manner only in the high resolution ocean versions of the model. This feature clearly emphasizes the role of the ocean. In addition we know that only the high resolution atmosphere can capture correctly the NAO pattern and its variability and this seems to be reflected in the different atmospheric patterns of HH and HL (although part of this difference may reflect the lack of sufficiently long time series).

5 Summary and discussion

In this paper, different resolutions of the coupled ocean-atmosphere general circulation model of IPSL are used to study the effect of horizontal resolution in simulating climate variability. We concentrate on simulated climate variability at inter-annual and inter-decadal scales, mainly in sea surface temperatures. A statistical method, called the Multi-Channel Singular Spectrum Analysis (M-SSA), is used to extract consistent oscillating patterns from the simulations. We can detect and then reconstruct oscillations (as defined by Vautard et al. 1992) corresponding to a precise period. Composite maps are thus obtained in which we can follow the evolution of the SST anomalies during a cycle.
Global simulated SST standard deviation maps, compared with GISST2 observations, indicate the importance of a high resolution ocean to simulate a more realistic inter-annual SST variability.
Simulated El-Niño-like oscillation in the tropical Pacific is too confined at the equator and is propagating too far westward, compared with GISST2 observations, whatever the resolution of the model. The sea level pressure (SLP) EOFs patterns for the northern hemisphere are best simulated in HH than in LL, and the percentages of variance are higher (not shown).
In the North Atlantic area, the coupled model simulates a winter quasi-decadal SST oscillation, whatever the resolution, like in the observations. The spatial structure associated to some of the phases of the HH quasi-decadal SST oscillation looks like structures obtained from an analysis of the observations, with in particular the presence of a sea surface temperature tripole structure. HL simulates also a decadal oscillation with the presence of this SST tripole. A high resolution ocean seems to be important to simulate a realistic variability when we compare the spatial structures of these oscillations with GISST2 oscillation, because LL is less successful.
The association of atmospheric and oceanic anomalies appears similar to the observations only in the short HH simulation: longer experiments are required to fully ascertain this link, and determine whether it is a coupled mode, or the response of one component to the other. In spite of our short simulation, we try to get some insight into the mechanisms of this quasi-decadal SST oscillation in the North Atlantic and we focus on the HH one, where the signal seems to propagate. Composite maps of atmospheric surface fields (like SLP and wind stress) are made for Phase 6 of this SST oscillation. The SLP distribution presents a North-South dipole, which is similar to the positive phase of the North Atlantic Oscillation (NAO) index. The NAO mode is the most important structure of bimodal variability in the North Atlantic. Wind stress follows the subtropical gyre movement during this phase. This SLP structure associated to the SST tripole is also found in observations when we calculate the correlation coefficient in winter between GISST2 observations and NAO index, defined by Hurrell (1995) as normalized SLP differences between Portugal and Iceland. The comparison of the simulation at different resolutions are indicating the essential role of a "high" resolution ocean to solve out the structure of the anomalies in the North Atlantic.

Acknowledgments. The authors thank particularly Robert Vautard for initiating the first author to the Multi-Channel Singular Spectrum Analysis and Guy Plaut for giving her advice about the use of this method. The authors are also grateful to Olivier Marti and three internal reviewers: Pascale Braconnot, Pascal Yiou and Philippe Courtier for their useful comments and discussions. Two of the three coupled simulations (HH and HL) were carried out by Laurent Fairhead on the Cray C-98 of the Institut de Recherche en Informatique Scientifique (IDRIS) of the Centre National de Recherche Scientifique (CNRS), and the other one (LL) was carried out at the Laboratoire des Sciences du Climat et de l'Environnement (LSCE) by Pascale Braconnot and Olivier Marti. These simulations have been run with the support of the EC Project SIDDACLICH.

name of the simulation	LL	HH	HL
atmospheric version	LMD5.3	LMD5.3	LMD5.3
number of atmospheric points in longitude	64	96	64
number of atmospheric points in latitude	50	72	50
number of atmospheric points in vertical	11	15	15
oceanic version	OPA7G2	OPA7G2	OPAICE
number of oceanic points in longitude	92	182	182
number of oceanic points in latitude	76	152	152
number of oceanic points in vertical	30	31	31
version of the coupler	OASIS2.0	OASIS2.0	OASIS 2.1
length of the simulation	100 years	25 years	100 years
initial atmospheric conditions	climatological run (Reynolds SST)	AMIP run	AMIP run
initial oceanic conditions	10-year forced run (Hellerman winds, Esbensen-Kushnir fluxes)	restart from Levitus	Levitus
solar constant ($W.m^{-2}$)	1365	1367	1367
atmospheric diffusion threshold	$10^{-7}m^2.s^{-2}$	$10^{-8}m^2.s^{-2}$	$10^{-8}m^2.s^{-2}$
hot cloudy droplet size	$10\mu m$	$15\mu m$	$15\mu m$
long-wave radiation scheme	Morcrette's scheme (1990)	modified version of the Morcrette's scheme (see text)	modified version of the Morcrette's scheme (see text)
temperature threshold for ice clouds	-	-	diminution

Table 1: Short description of the 3 runs used with the principal differences between the versions, a "Low" resolution atmosphere coupled to a "Low" resolution ocean (LL), a "High" resolution atmosphere coupled to a "High" resolution ocean (HH) and a "Low" resolution atmosphere coupled to a "High" resolution ocean (HL). (AMIP : Atmospheric Models Intercomparison Project, SST : Sea Surface Temperature).

window	72 months			120 months			168 months		
M-SSA	pair	%	period	pair	%	period	pair	%	period
LL	5-6	6	96	**6-7**	**4**	**100**	6-7	4	200
	9-10	3	42	10-11	3	40	10-11	3	40
HH	1-2	37	111	1-2	38	125	simulation too short		
	7-8	8	23	9-10	8	25	-		
GISST2	**1-2**	**22**	**50**	1-2	15	50	3-4	11	50
	7-8	8	28	10-11	5	30	9-10	7	125

Table 2: Main characteristics of the oscillating pairs identified by the M-SSA on monthly sea surface temperature for **world ocean** , for LL (80 years), HH (17 years) and GISST2 observations (1950-1994) interpolated on the HH atmospheric grid (96 points in longitude and 72 points in sine of the latitude), in first column. Three main windows are used: 72 months, 120 months and 168 months. Results are obtained with 5 channels retained for the global study. Each column of window contains the pair order, the variance of the oscillating pair (%) and the main peak period (in months). Numbers in bold type correspond to the reconstructed pairs for the following graphs.

window	72 months			120 months		
M-SSA	pair	%	period	pair	%	period
LL	**3-4**	**14.3±1.2**	**45.3±1.2**	3-4	11±0.8	44±0.9
HH	**1-2**	**21±2**	**32.5±0.4**	2-3	16.6±1.2	30.6±0.5
	5-6	10.3±0.4	16.6±0.4	5-6	11±0.8	40.3±0.5
	-			7-8	7.3±0.5	16.7±0.2
GISST2	**1-2**	**22±1.6**	**61±1.4**	1-2	14.6±0.9	59
	5-6	10.3±0.5	28.3±0.5	8-9	6.3±0.5	29

Table 3: Main characteristics of the oscillating pairs identified by the M-SSA on monthly sea surface temperature for the **tropical Pacific** (20^oN-20^oS;120^oE-90^oW), for LL (80 years), HH (17 years) and GISST2 observations (1903-1994) on the original grid $1^o * 1^o$, in first column. Two main windows are used: 72 months and 120 months. Each column of window contains the pair order, the variance of the oscillating pair (%) and the main peak period (in months). These results are obtained with three different tests on the number of S-PCs kept (number of channels c): c=5, c=7 and c=10. Numbers in bold type correspond to the reconstructed pairs for the following graphs.

window	6 years			10 years			14 years		
M-SSA	pair	%	period	pair	%	period	pair	%	period
LL	4-5	12±1	3.7	2-3	13	12	2-3	10±0.8	13±0.6
	7-8	9±0.8	3.5±0.2		-		4-5	7.8±0.6	7.8±0.3
		-			-		6-7	7.5±0.5	3.5±0.05
HH	window too short			1-2	24	10	2-3	23	8.4
GISST2	3-4	16±1.2	4.5±0.3	4-5	11±0.8	4,7±0.2	4-5	9.3±0.8	5.2±0.2
		-			-		7-8	7.6±0.5	4.2±0.2

Table 4: Main characteristics of the oscillating pairs identified by the M-SSA on winter sea surface temperature for the **North Pacific** (0^oN-70^oN;120^oE-90^oW,DJF), for LL (79 winters), HH (16 winters) and GISST2 observations (1904-1992) on the original grid $1^o * 1^o$, in first column. Three main windows are used: 6 years, 10 years and 14 years. Each column of window contains the pair order, the variance of the oscillating pair (%) and the main peak period (in years). These results are obtained with three different tests on the number of S-PCs kept (number of channels c): c=5, c=7 and c=10.

window	6 years			10 years			14 years		
M-SSA	pair	%	period	pair	%	period	pair	%	period
LL	8-9	5	3.2	7-8	5	9.5	**7-8**	**5**	**10.6**
HH	1-2	36±3.2	11±2.3	**1-2**	**36±1.7**	**8**	simulation too short		
GISST2	**4-5**	**11.5±1.2**	**8.3**	3-4	13±1	13	3-4	12	13
		-			-		5-6	8	7.4

Table 5: Main characteristics of the oscillating pairs identified by the M-SSA on winter sea surface temperature for the **North Atlantic** (15^oN-70^oN;75^oW-20^oE, DJF), for LL (79 winters), HH (16 winters) and GISST2 observations (1904-1992) on the original grid $1^o * 1^o$, in first column. Three main windows are used: 6 years, 10 years and 14 years. Each column of window contains the pair order, the variance of the oscillating pair (%) and the main peak period (in years). These results are obtained with three different tests on the number of S-PCs kept (number of channels c): c=5, c=7 and c=10. Numbers in bold type correspond to the reconstructed pairs for the following graphs.

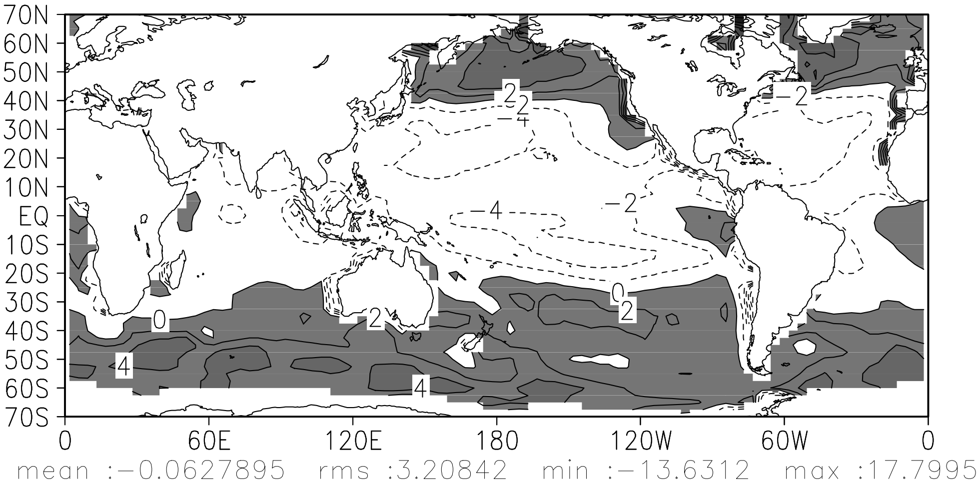

Figure 1: *Coupled sea surface temperature (first five years) minus Reynolds data (1985-1990) for LL in July. Shaded regions correspond to positive values. Contour interval : 2^oC.*

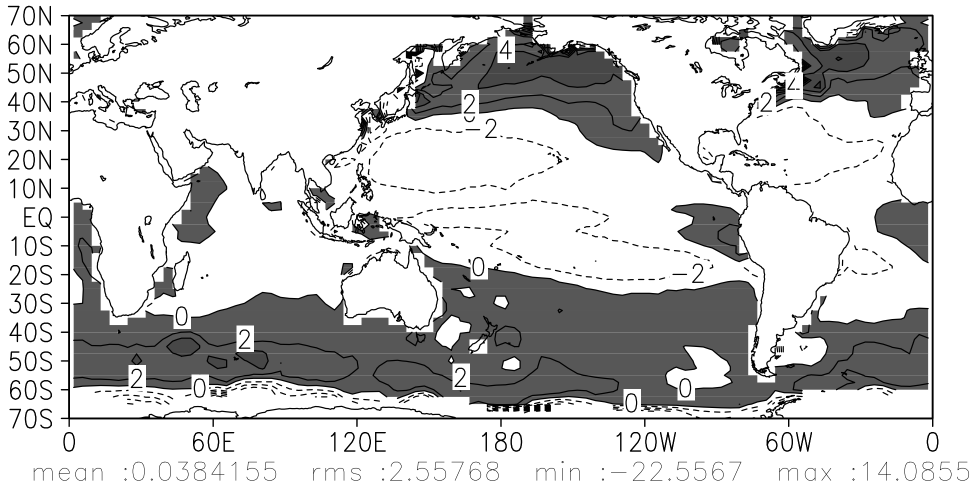

Figure 2: *Coupled sea surface temperature (first five years) minus Reynolds data (1985-1990) for HH in July. Shaded regions correspond to positive values. Contour interval : 2^oC. The tropical zone (30^oS-30^oN) is too cold of about 2^oC. On the contrary, high latitudes are too hot compared with observations.*

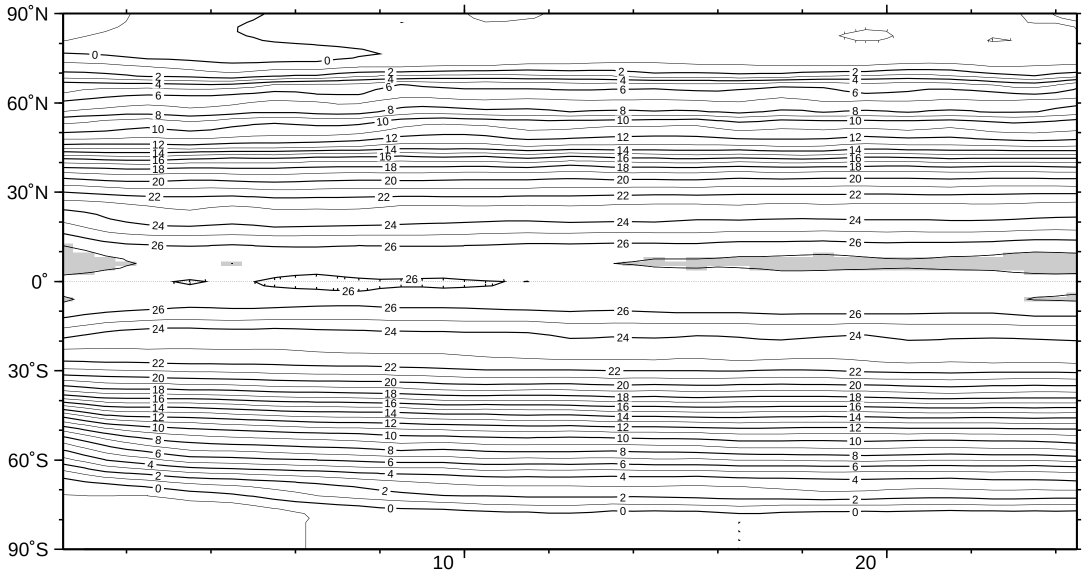

Figure 3: *Latitude-time diagram of the zonally averaged annual sea surface temperature (SST) over the 25 simulated years of HH. Shaded regions correspond to values greater than 27°C. Contour interval : 1°C.*

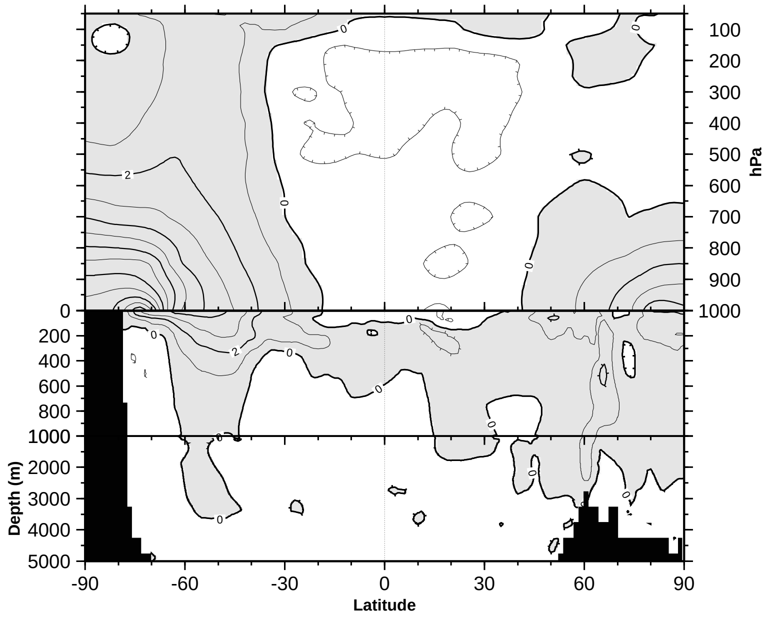

Figure 4: *Zonal mean of the difference of temperature of year 15 minus year 1 for HH. Shaded regions correspond to positive values. Contour interval : 1°C in atmosphere and in ocean. A zoom is made on the first 1000 meters of the ocean.*

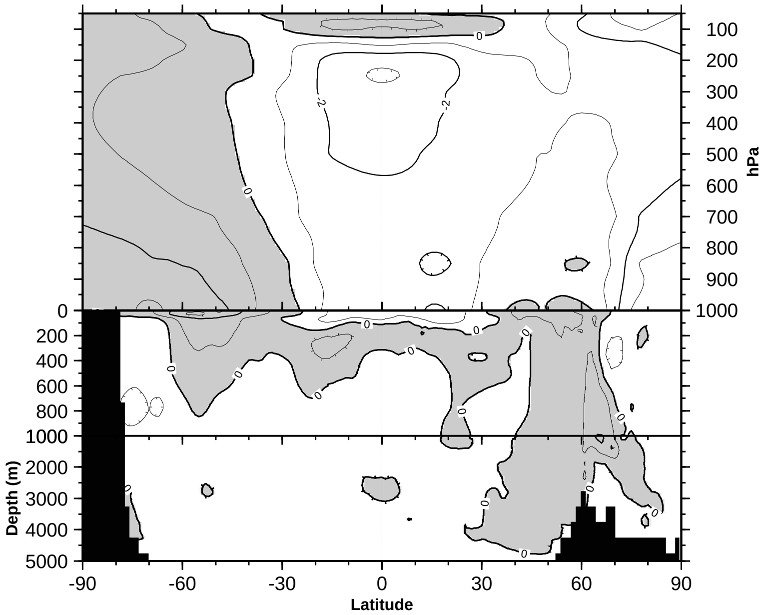

Figure 5: *Zonal mean of the difference of temperature of year 22 minus year 8 (the last forced year towards climatology) for HL. Shaded regions correspond to positive values. Contour interval : 1°C in atmosphere and in ocean. A zoom is made on the first 1000 meters of the ocean.*

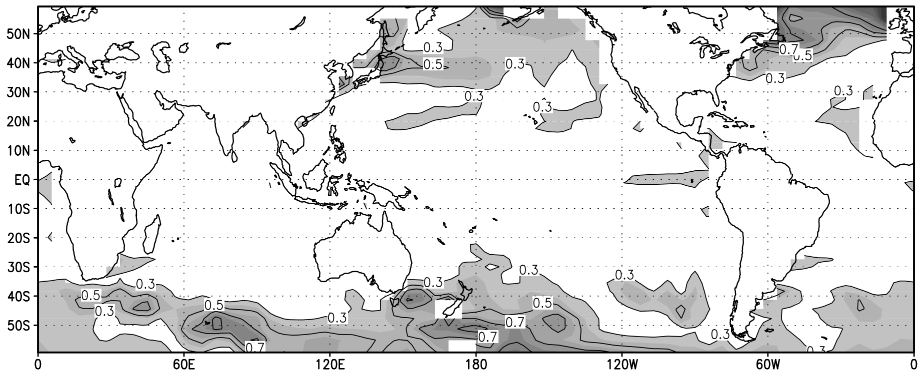

Figure 6: *Root-mean square (rms) calculated for monthly sea surface temperatures for LL. The mean annual cycle was removed from data. Root-mean square was calculated for the last 80 years of the run, in the latitude band of* 60^oN *and* 60^oS*. Shaded regions correspond to values greater than 0.3. Contour interval :* 0.2.

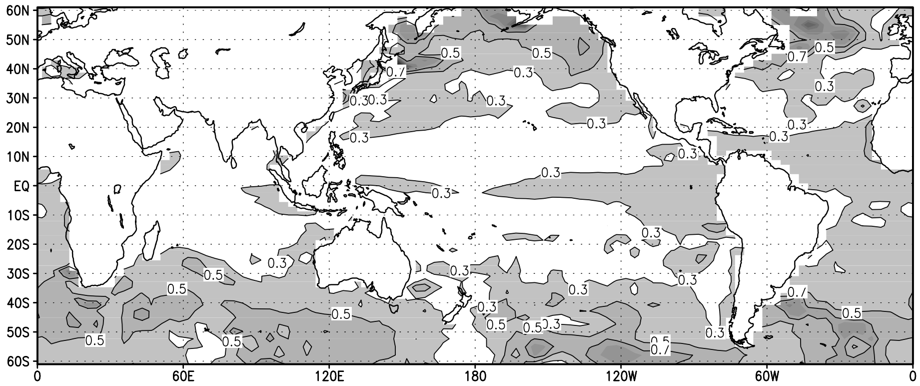

Figure 7: *Root-mean square (rms) calculated for monthly sea surface temperatures for HH. The mean annual cycle was removed from data. Root-mean square was calculated for the last 19 years of the run, in the latitude band of* 60^oN *and* 60^oS*. Shaded regions correspond to values greater than 0.3. Contour interval :* 0.2.

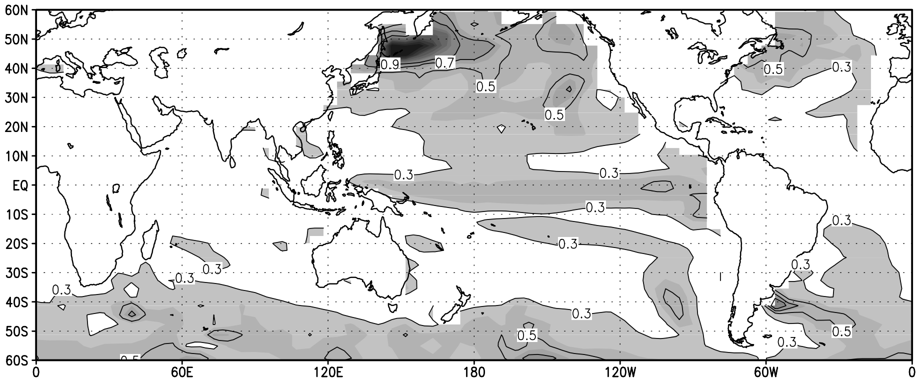

Figure 8: *Root-mean square (rms) calculated for monthly sea surface temperatures for HL. The mean annual cycle was removed from data. Root-mean square was calculated for 69 years of the run, starting at year 30, in the latitude band of* $60^{o}N$ *and* $60^{o}S$*. Shaded regions correspond to values greater than 0.3. Contour interval :* 0.2.

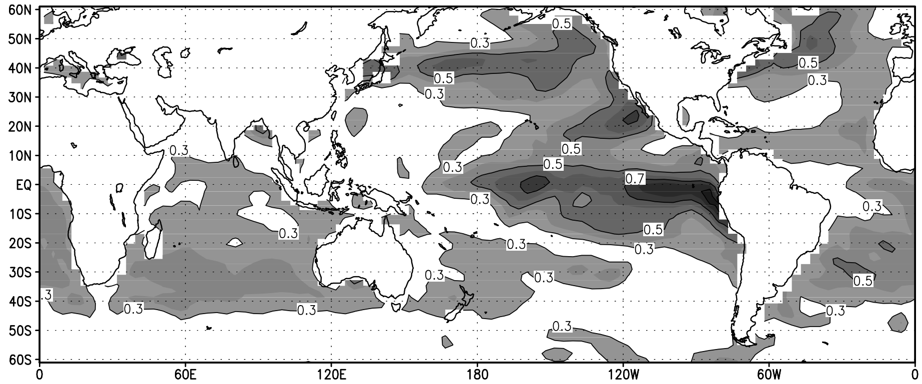

Figure 9: *Root-mean square (rms) calculated for monthly sea surface temperatures for GISST2 observations interpolated on the high resolution atmospheric grid. The mean annual cycle was removed from data. Root-mean square was calculated for the period 1950-1994, in other words for 45 years of observations, in the latitude band of* $60^{o}N$ *and* $60^{o}S$*. Shaded regions correspond to values greater than 0.3. Contour interval :* 0.2.

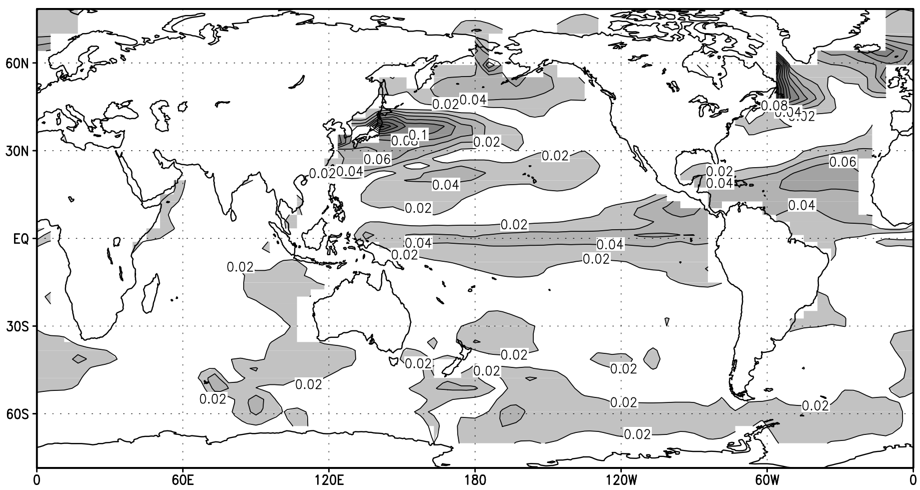

Figure 10: *Root-mean square (rms) calculated for ST-RCs 6-7 (c=5,w=120) of monthly sea surface temperatures for LL. The mean annual cycle and a seasonal trend have been removed from data. Shaded regions correspond to values greater than 0.02. Contour interval :* 0.02.

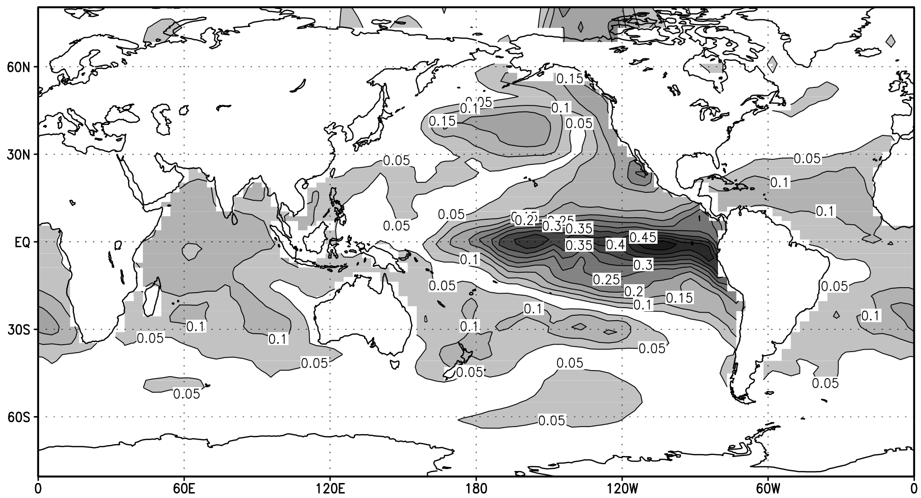

Figure 11: *Root-mean square (rms) calculated for ST-RCs 1-2 (c=5,w=72) of monthly sea surface temperatures for the 45-year GISST2 observations (1950-1994) interpolated on the HH atmospheric grid (96 points in longitude and 72 points in sine of the latitude). The mean annual cycle and a seasonal trend have been removed from data. Shaded regions correspond to values greater than 0.05. Contour interval :* 0.05.

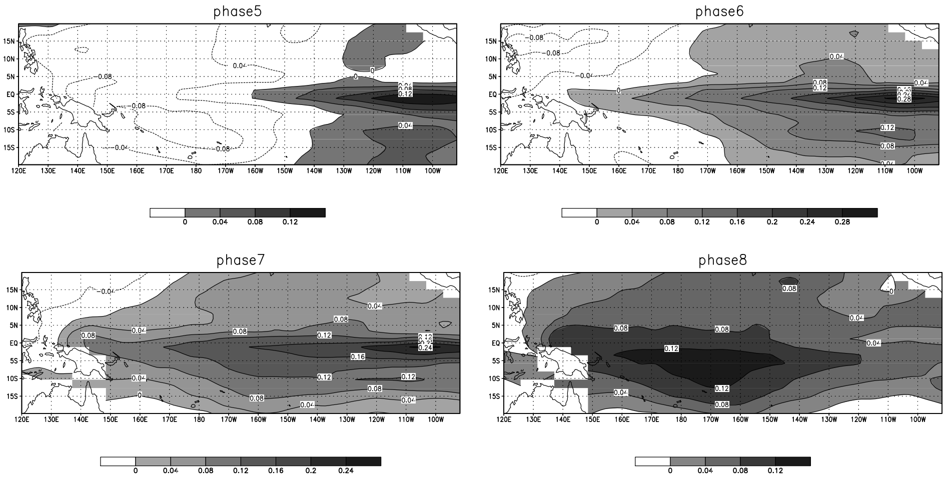

Figure 12: *Reconstructed cycle (w=72 months, c=10) of the El-Niño oscillation (period of about 47 months, 13%) for LL sea surface temperature in the tropical Pacific (20°N-20°S). It is based on ST-RCs 3-4. Shaded regions correspond to positive values. Contour interval :* 0.04°C*. A linear trend has been removed from data. 8 phase-composites are obtained. Phase-composites 5 to 8 are plotted in this figure. Phase-composites 1 to 4 are respectively similar to phase-composites 5 to 8 but with signs reversed (not shown).*

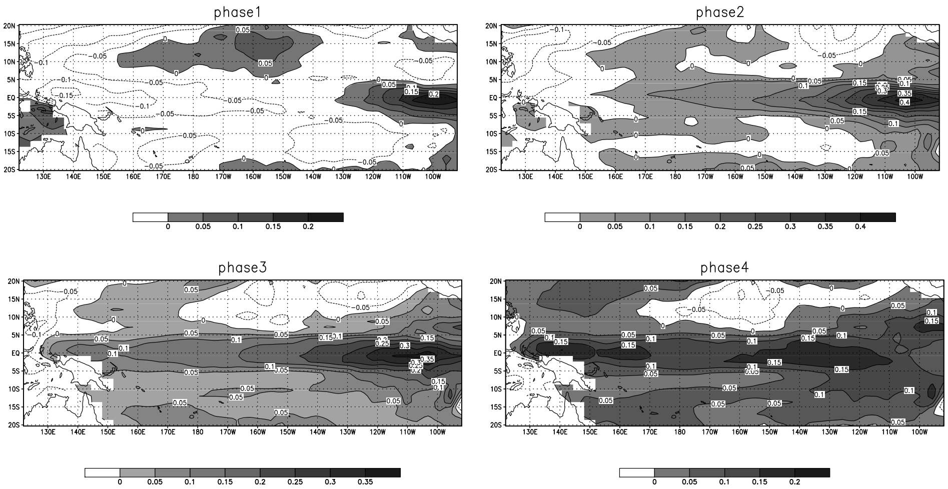

Figure 13: *Reconstructed cycle (w=72 months, c=10) of the El-Niño oscillation (period of about 33 months, 20%) for HH sea surface temperature in the tropical Pacific (20°N-20°S). It is based on ST-RCs 1-2. Shaded regions correspond to positive values. Contour interval :* 0.05°C*. The eight first years of the run and a linear trend have been removed from data. 8 phase-composites are obtained. Phase-composites 1 to 4 are plotted in this figure. Phase-composites 5 to 8 are respectively similar to phase-composites 1 to 4 but with signs reversed (not shown).*

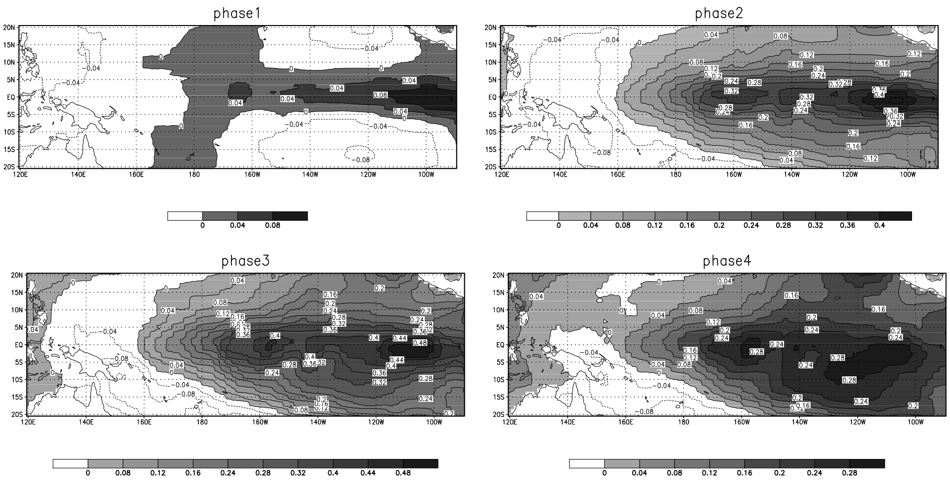

Figure 14: *Reconstructed cycle (w=72 months, c=5) of the El-Niño oscillation (period of about 62 months, 24%) for GISST2 sea surface temperatures (1903-1994) in the tropical Pacific (*20^oN*-*20^oS*). It is based on ST-RCs 1-2. Shaded regions correspond to positive values. Contour interval :* 0.04^oC*. A linear trend has been removed from data. 8 phase-composites are obtained. Phase-composites 1 to 4 are plotted in this figure. Phase-composites 5 to 8 are respectively similar to phase-composites 1 to 4 but with signs reversed (not shown).*

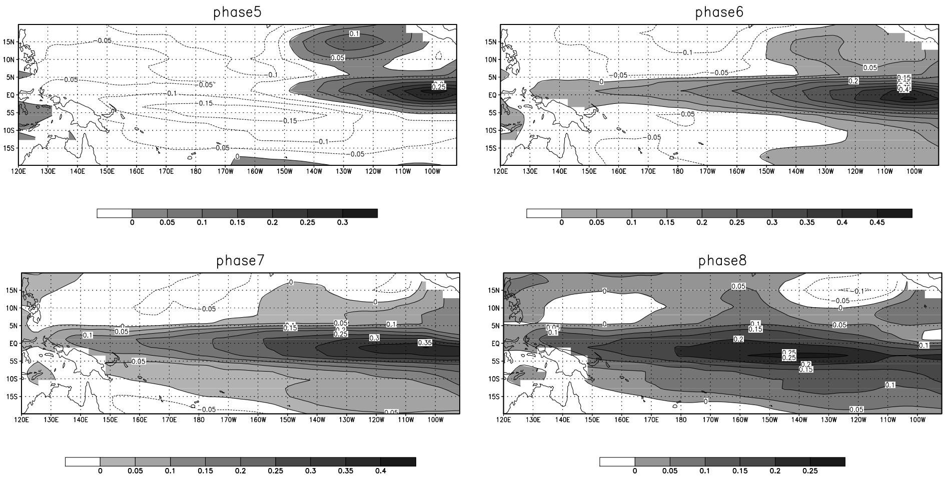

Figure 15: *Reconstructed cycle (w=72 months, c=5) of the El-Niño oscillation (period of about 36 months, 22%) for HL sea surface temperature (years 30 to 98) in the tropical Pacific (*20^oN*-*20^oS*). It is based on ST-RCs 2-3. Shaded regions correspond to positive values. Contour interval :* 0.05^oC*. 8 phase-composites are obtained. Phase-composites 5 to 8 are plotted in this figure. Phase-composites 1 to 4 are respectively similar to phase-composites 5 to 8 but with signs reversed (not shown).*

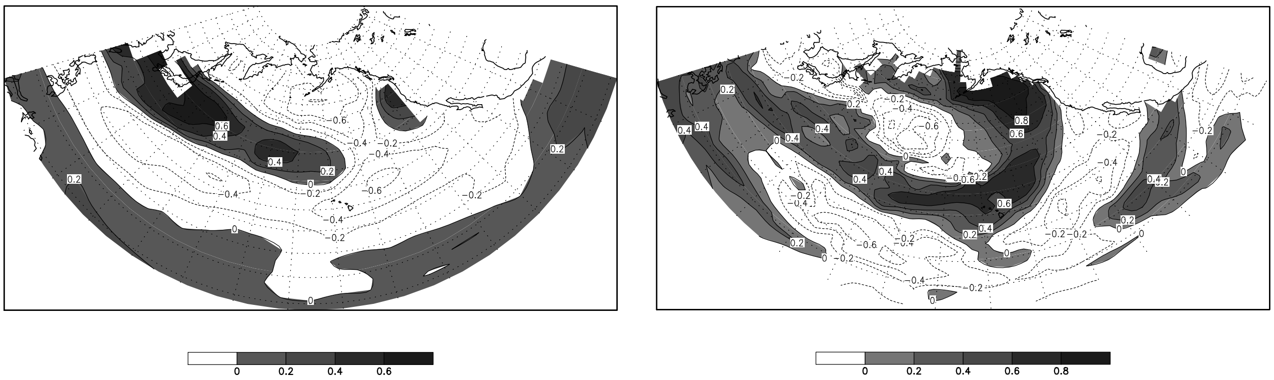

(a) and (b)

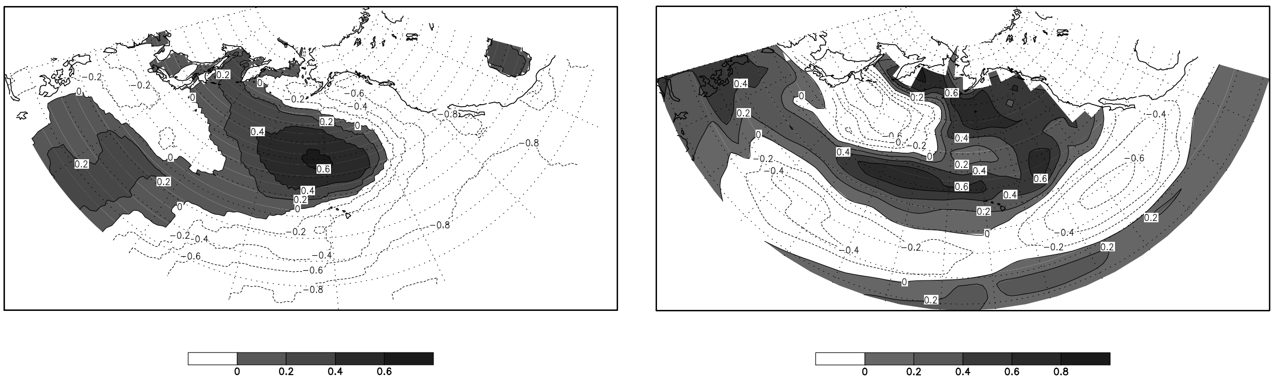

(c) and (d)

Figure 16: *First Empirical Orthogonal Function (EOF1) of sea surface temperature in the North Pacific (0^oN-70^oN) and for winter (DJF). A linear trend has been removed from data. Values are correlation coefficients. Contour interval :* 0.2*. Shaded regions correspond to positive values. (a) for the last 80 years of LL. This EOF represents 18.7% of the total variance. (b) for the last 17 years of HH. This EOF represents 19.6% of the total variance. (c) for GISST2 observations (1904-1992, resolution $1^o * 1^o$). This EOF represents 25% of the total variance. (d) for 68 years of HL. This EOF represents 21.8% of the total variance.*

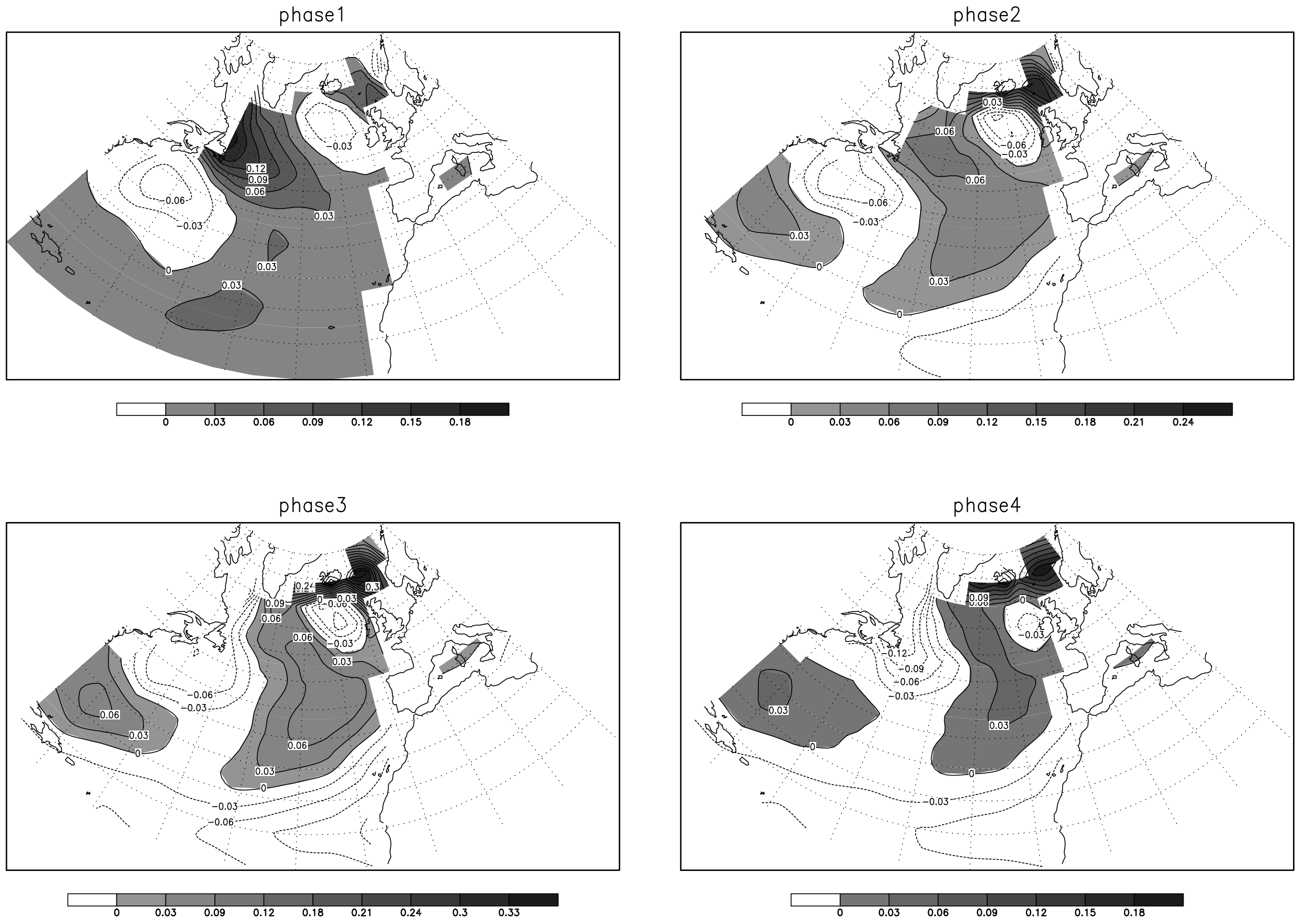

Figure 17: *Reconstructed cycle (w=14 years, c=5) of a 10-year oscillation (5%) for LL sea surface temperature, in the North Atlantic (15°N-70°N) and for winter (DJF). It is based on ST-RCs 7-8. Shaded regions correspond to positive values. Contour interval : 0.03°C. A linear trend has been removed from data. 8 phase-composites are obtained. Phase-composites 1 to 4 are plotted in this figure.*

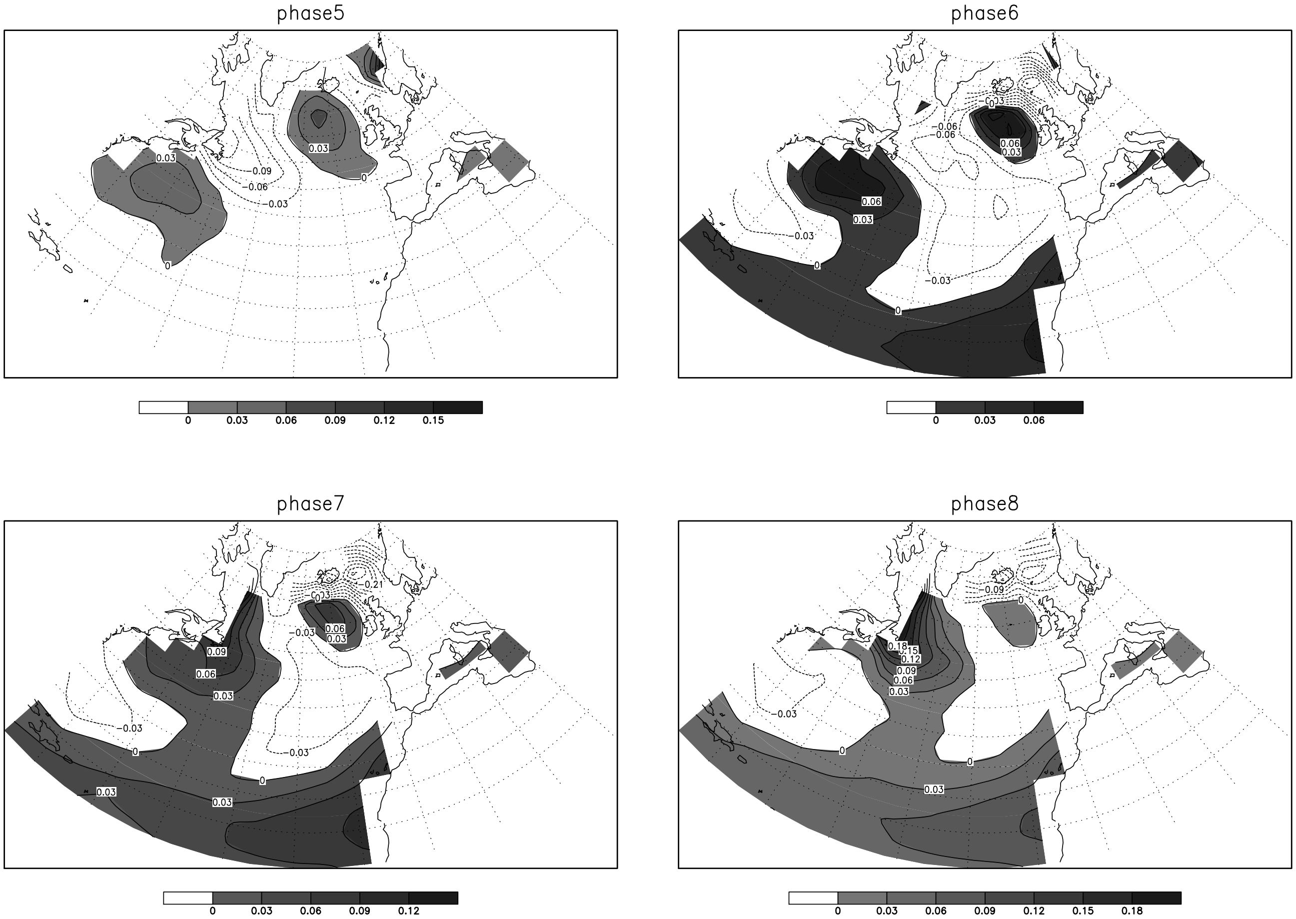

Figure 18: *Same figure than the previous one for phase-composites 5 to 8.*

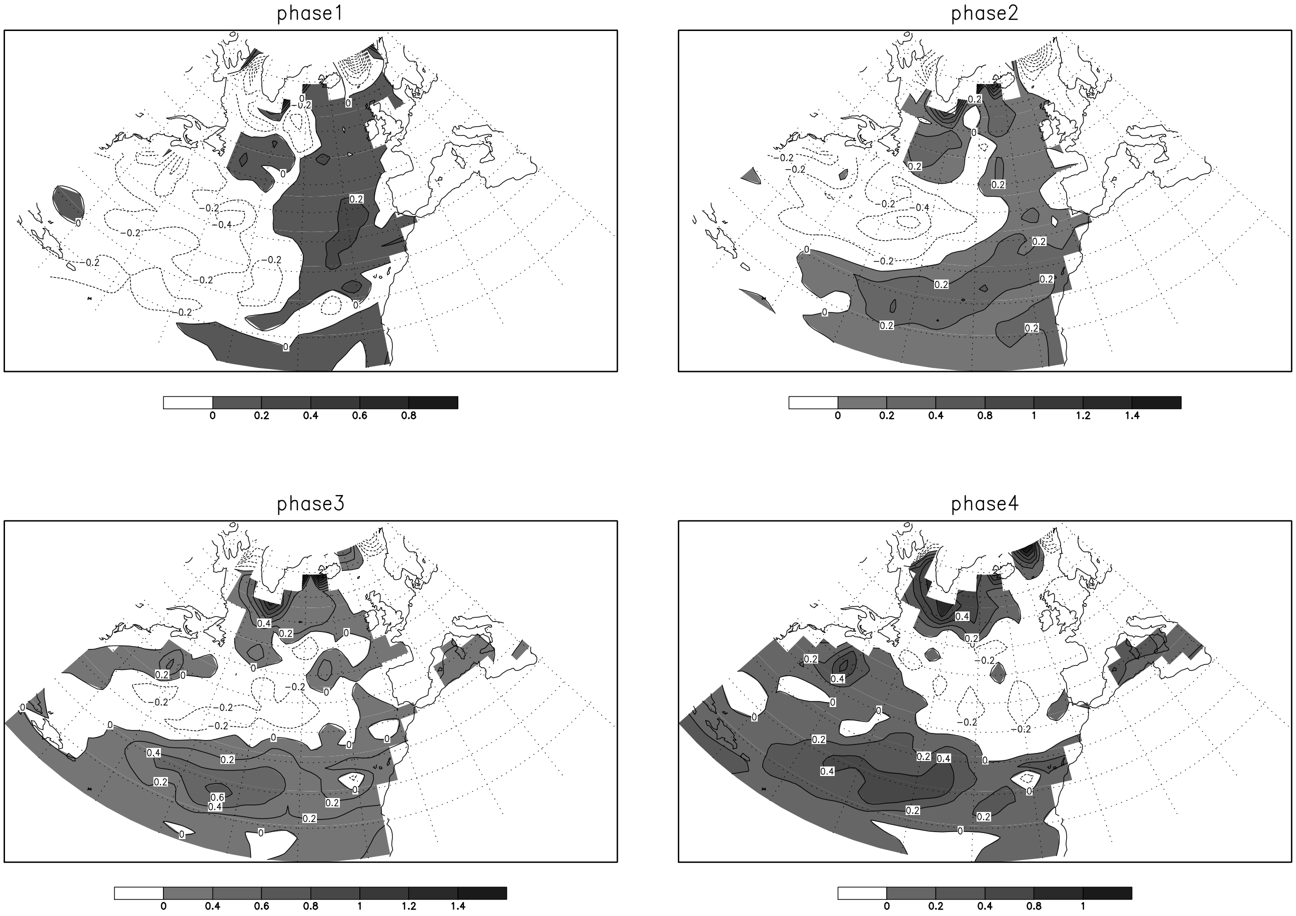

Figure 19: *Reconstructed cycle (w=10 years, c=5) of a 8-year oscillation (39%) for HH sea surface temperature, in the North Atlantic (15^oN-70^oN) and for winter (DJF). It is based on ST-RCs 1-2. Shaded regions correspond to positive values. Contour interval : 0.2^oC. A linear trend has been removed from data. 8 phase-composites are obtained. Phase-composites 1 to 4 are plotted in this figure.*

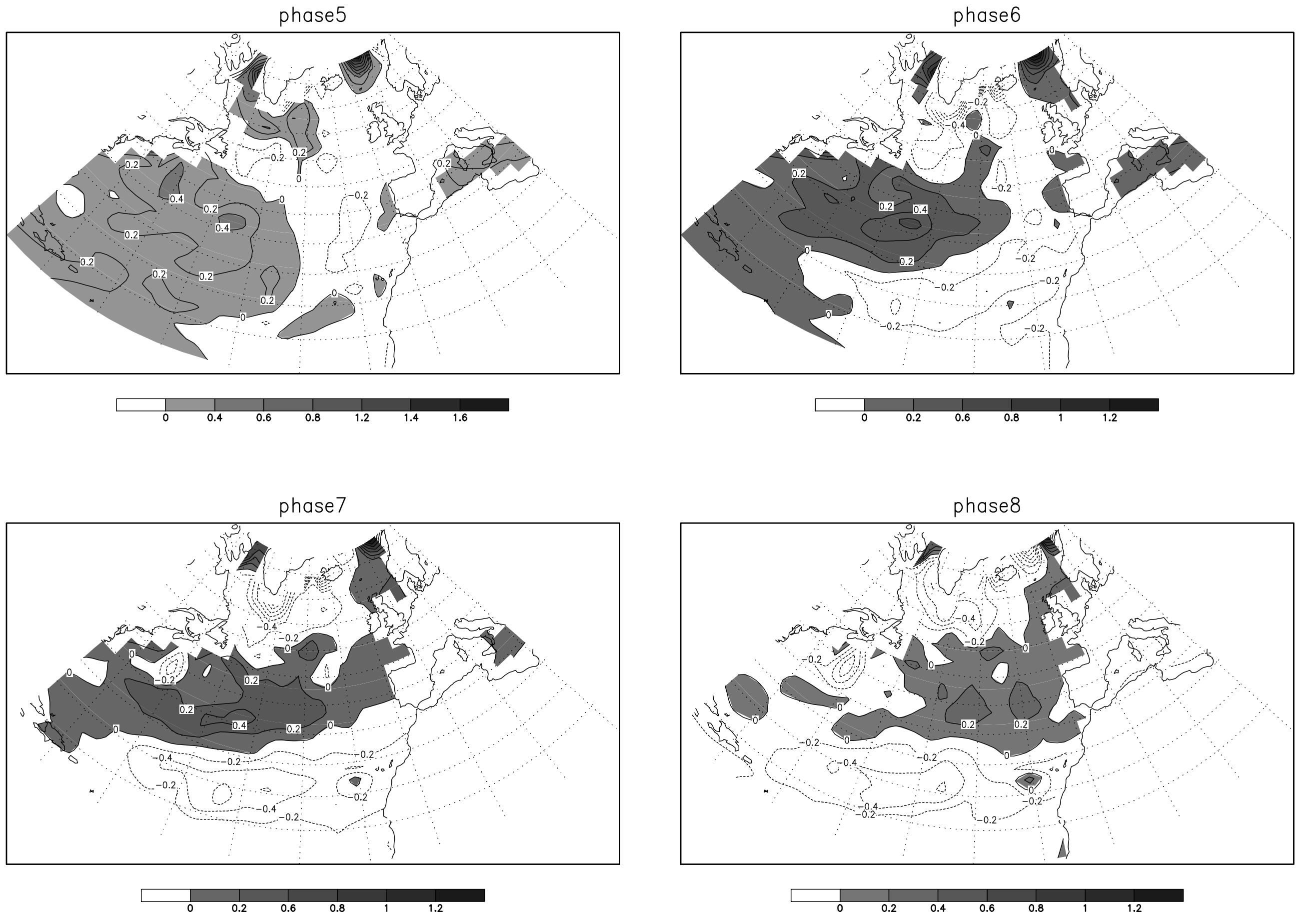

Figure 20: *Same figure than the previous one for phase-composites 5 to 8.*

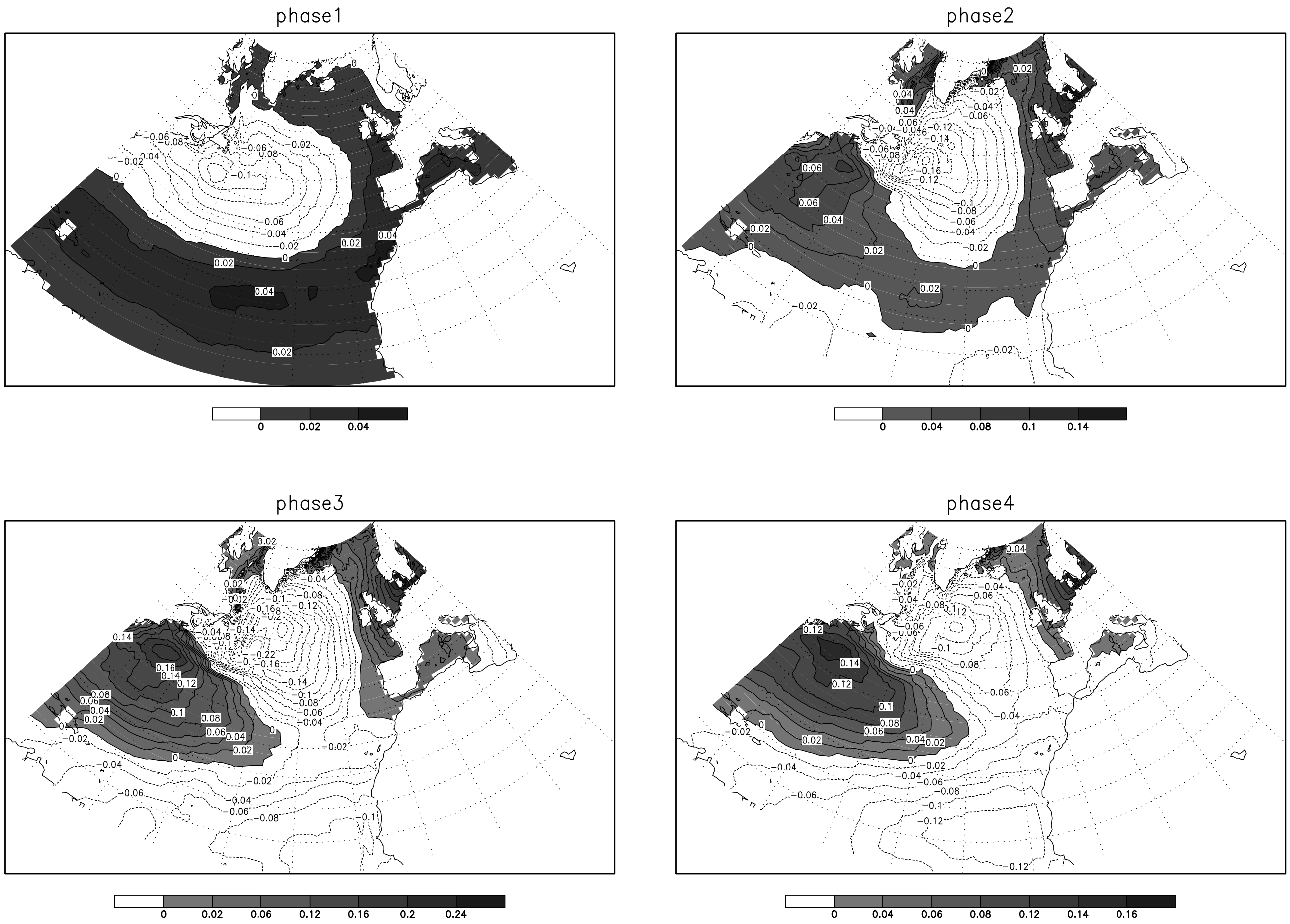

Figure 21: *Reconstructed cycle (w=6 years, c=5) of a 8.3-year oscillation (13%) for the GISST2 sea surface temperatures (1904-1992, resolution* $1^o * 1^o$*), in the North Atlantic (*$15^o N$*-*$70^o N$*) and for winter (DJF). It is based on ST-RCs 4-5. Shaded regions correspond to positive values. Contour interval :* $0.02^o C$*. A linear trend has been removed from data. 8 phase-composites are obtained. Phase-composites 1 to 4 are plotted in this figure.*

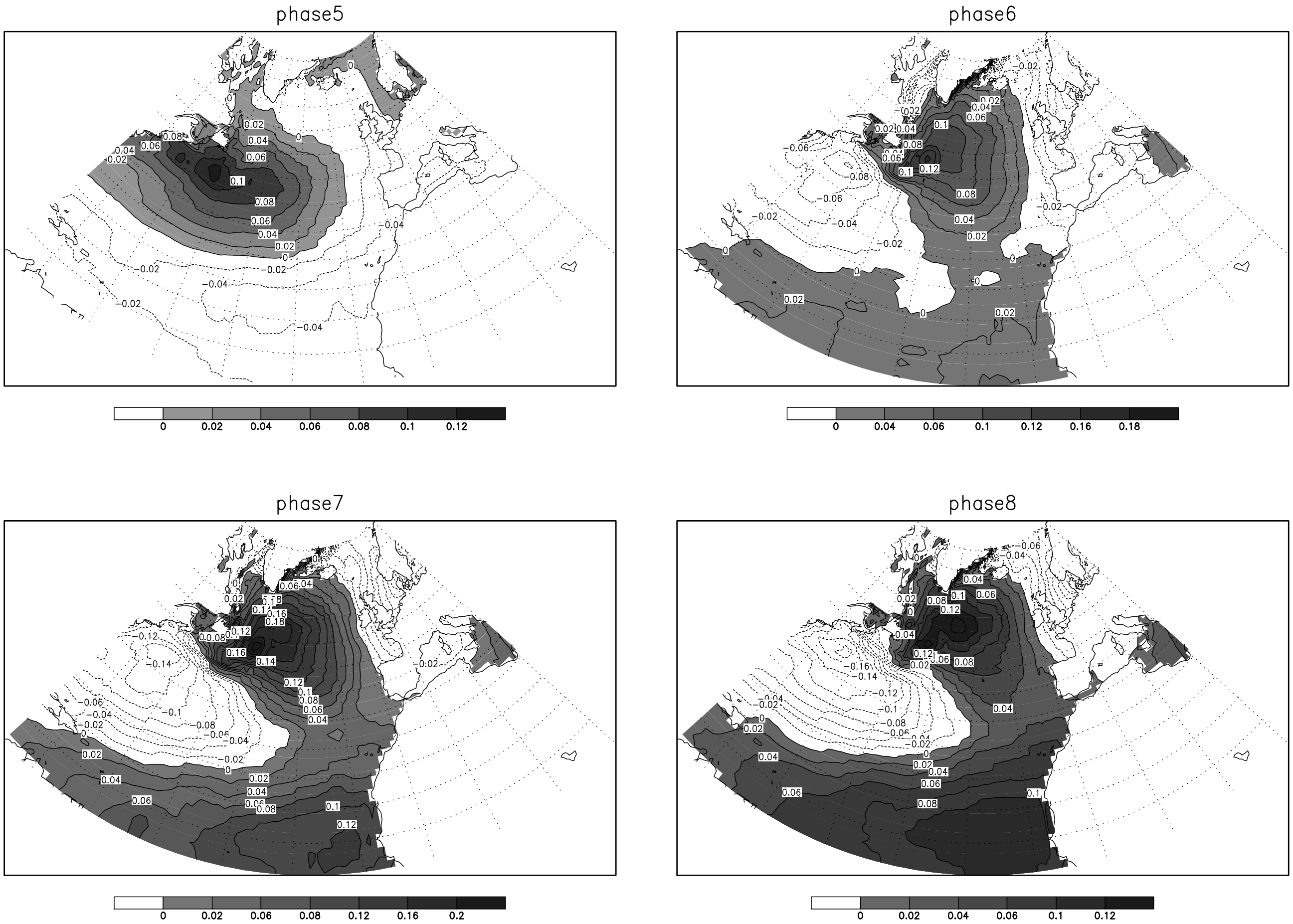

Figure 22: *Same figure than the previous one for phase-composites 5 to 8.*

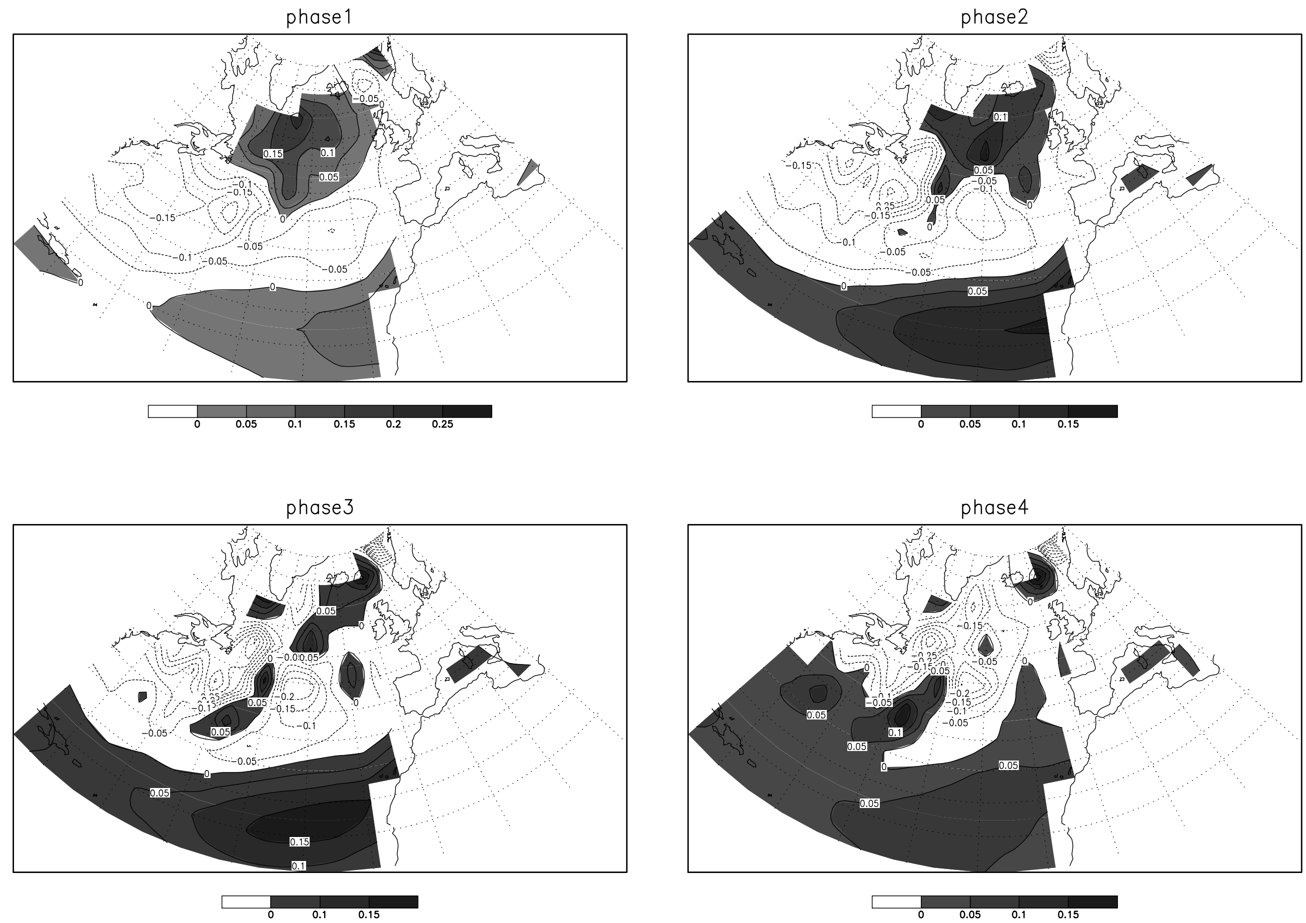

Figure 23: *Reconstructed cycle (w=6 years, c=5) of a 12-year oscillation (22%) for winter sea surface temperatures in HL, in the North Atlantic (15°N-70°N). It is based on ST-RCs 2-3. Shaded regions correspond to positive values. Contour interval : 0.05°C. A linear trend has been removed from data. 8 phase-composites are obtained. Phase-composites 1 to 4 are plotted in this figure.*

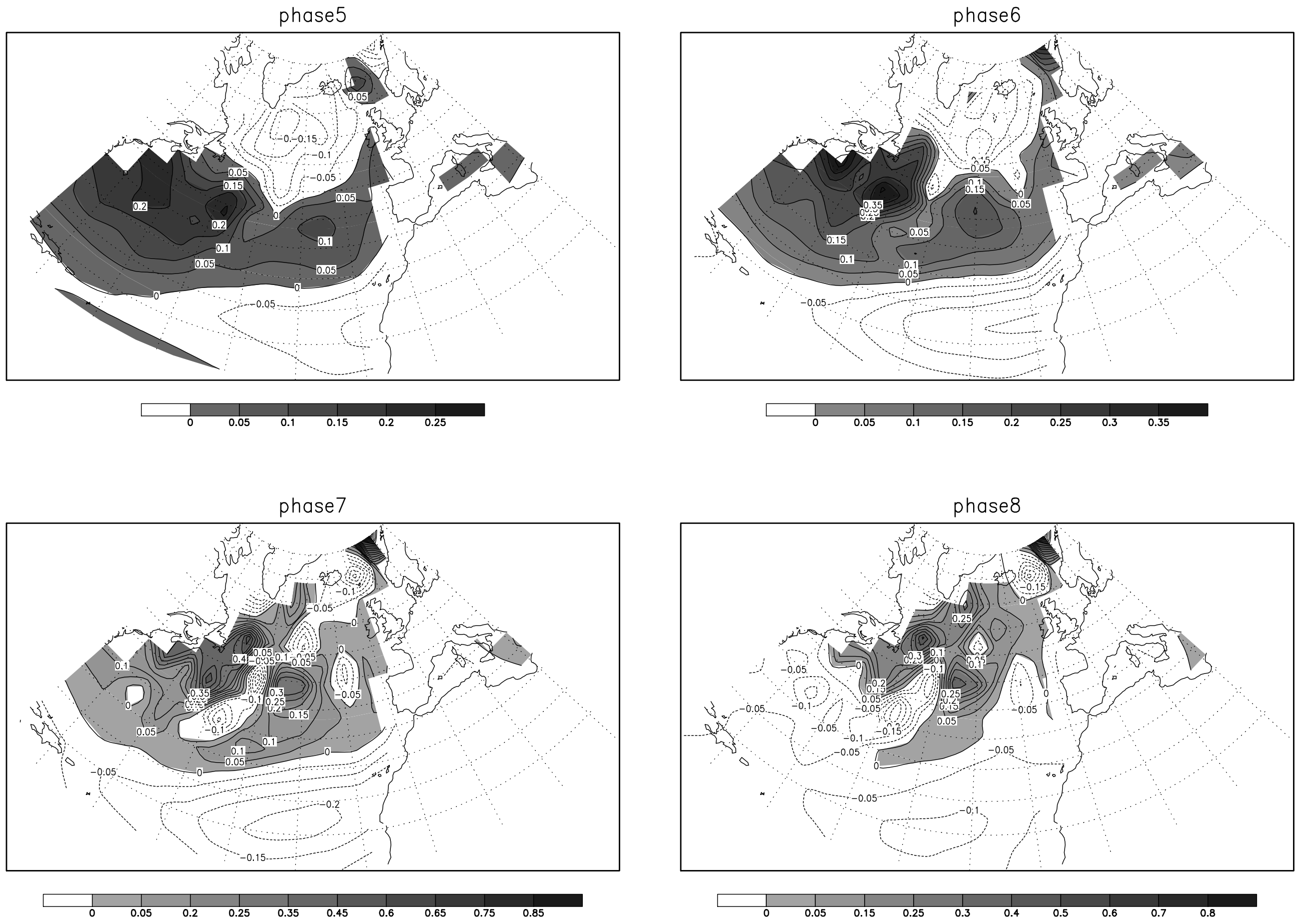

Figure 24: *Same figure than the previous one for phase-composites 5 to 8.*

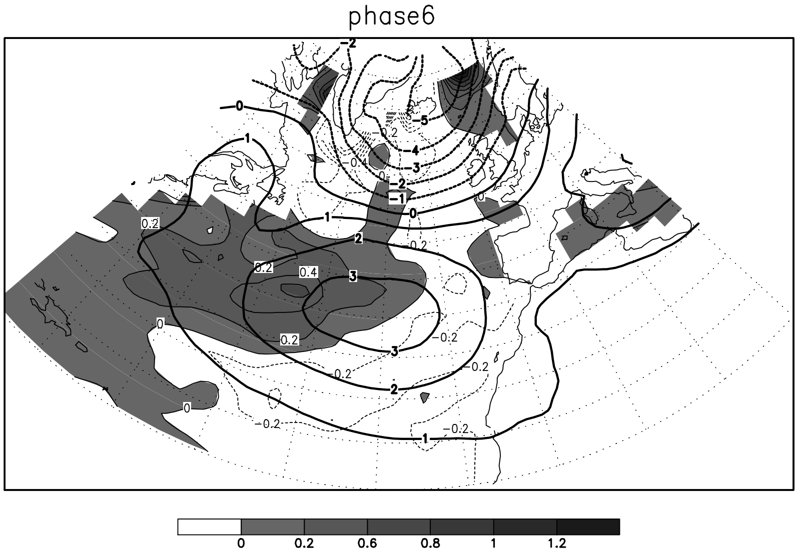

Figure 25: *Winter sea surface temperature (SST), in shaded areas, and sea-level pressure (SLP), in thick lines, during Phase 6 of the 8-year cycle obtained for sea surface temperature in HH (see figure 20), in the North Atlantic (15^oN-70^oN). Shaded regions correspond to positive SSTs and contour interval is* 0.2^oC. *Superposed to SST, sea-level pressure (SLP) is drawn in thick lines, with 1mb contour interval. It shows the behaviour of the atmosphere during Phase 6 of the 8-year SST oscillation.*

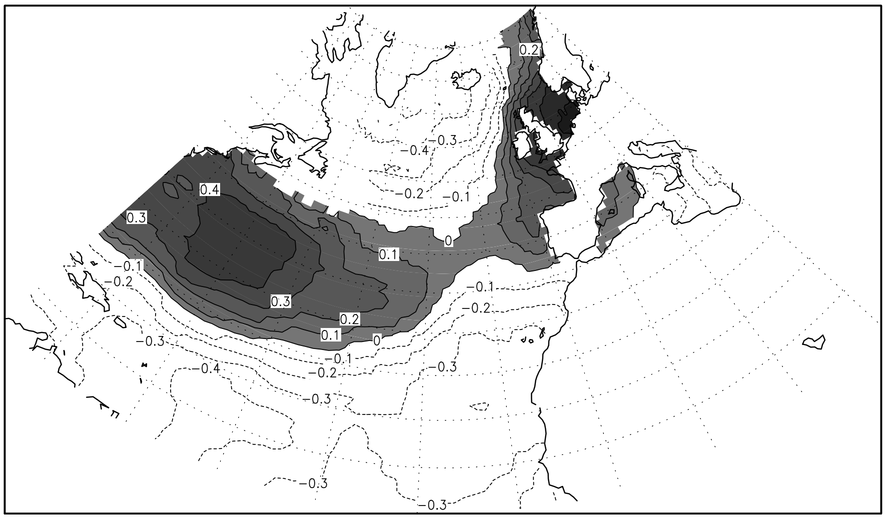

Figure 26: *Correlation coefficient for winter between GISST2 observations* ($1^o * 1^o$) *and NAO index (1903-1992) in North Atlantic* (15.5^oN-69.5^oN). *NAO index is defined by Hurrell, using normalized sea level pressure differences between Portugal and Iceland. Contour interval: 0.1. Shaded regions correspond to positive values.*

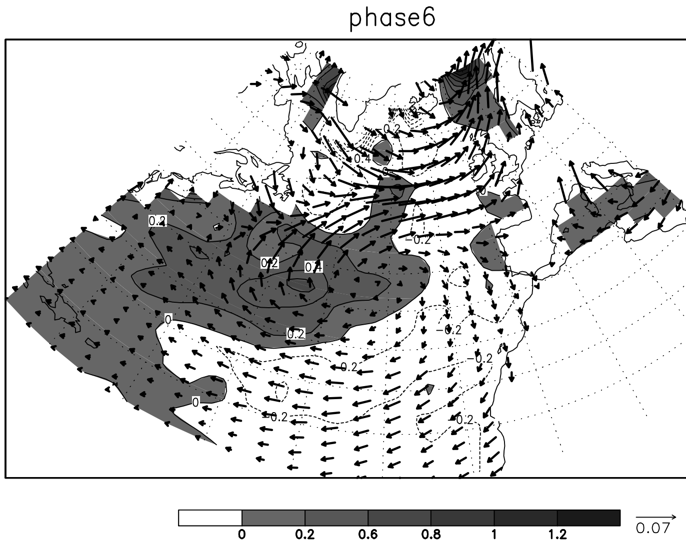

Figure 27: *Winter sea surface temperature (SST), in shaded areas, and wind stress, in thick arrows, during Phase 6 of the 8-year cycle obtained for sea surface temperature in HH (see figure 20), in the North Atlantic* (15^oN*-*70^oN*). Shaded regions correspond to positive SSTs and contour interval is* 0.2^oC*. Superposed to SST, stress wind vectors are drawn in thick lines* ($0.5cm = 0.07N.m^{-2}$*). It shows the behaviour of wind during Phase 6 of the 8-year SST oscillation.*

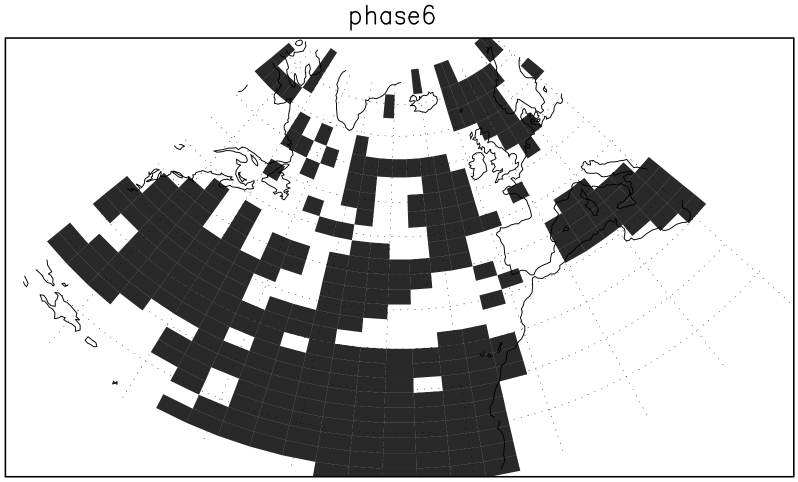

Figure 28: *Meshes of the grid where the winter SST anomalies* (^oC*) and the winter surface latent heat flux anomalies* ($W.m^{-2}$*) are of opposite signs, during Phase 6 of the 8-year HH sea surface temperature cycle.*

References

Bjerknes, J. (1964). Atlantic air-sea interaction. *Adv. in Geophys.*, 10:1–82.

Blanke, B. and Delecluse, P. (1993). Low frequency variability of the tropical Atlantic ocean simulated by a general circulation model with mixed layer physics. *J. Phys. Oceanogr.*, 23:1363–1388.

Braconnot, P., Marti, O., and Joussaume, S. (1997). Adjustment and feedbacks in a global coupled ocean-atmosphere model. *Climate Dyn.*, 13:507–519.

Broomhead, D. S. and King, G. P. (1986). On the qualitative analysis of experimental dynamical systems. In *Nonlinear Phenomena and Chaos.*, pages 113–144. Adam Hilger, Bristol.

Cayan, D. R. (1992). Latent and sensible heat flux anomalies over the northern oceans: driving the sea surface temperature. *J. Climate.*, 22:859–881.

Delecluse, P., Madec, G., Imbard, M., and Levy, C. (1993). OPA version 7, Ocean General Circulation Model, Reference Manual. Technical report, IPSL.

Delworth, T., Manabe, S., and Stouffer, R. J. (1993). Interdecadal variations of the thermohaline circulation in a Coupled Ocean-Atmosphere Model. *J. Climate.*, 6:1993–2011.

Fairhead, L., Dufresne, J. L., Le Treut, H., Li, Z. X., Grandpeix, J. Y., Forichon, M., Bony, S., Braconnot, P., Marti, O., Madec, G., Filiberti, M. A., Houssais, M. N., and Imbard, M. (1998). The IPSL coupled atmosphere-ocean GCM: description and climatology. *In preparation.*

Fouquart, Y. and Bonnel, B. (1980). Computation of solar heating of the Earth's atmosphere: a new parameterization. *Beitr. Phys. Atmos.*, 53:35–62.

Ghil, M. and Vautard, R. (1991). Interdecadal oscillations and the warming trend in global temperature time series. *Nature*, 350:324–327.

Graham, N. E., Barnett, T. P., Wilde, R., Ponater, M., and Schubert, S. (1994). On the roles of tropical and midlatitude SSTs in forcing interannual to interdecadal variability in the winter northern hemisphere circulation. *J. Climate.*, 7:1416–1441.

Grenier, H., Le Treut, H., and Fichefet, T. (1998). Tropical ocean-atmosphere interactions and climate drift in a 3-D climate model. *Submitted to Climate Dyn.*

Hansen, D. V. and Bezdek, H. F. (1996). On the nature of decadal anomalies in North Atlantic sea surface temperature. *J. Geophys. Res.*, 101:8749–8758.

Harzallah, A. and Sadourny, R. (1995). Internal versus SST-forced atmospheric variability as simulated by an atmospheric General Circulation Model. *J. Climate.*, 8:474–495.

Hurrell, J. W. (1995). Decadal trends in the North Atlantic Oscillation : regional temperatures and precipitation. *Science*, 269:676–679.

Hurrell, J. W. and Van Loon, H. (1997). Decadal variations in climate associated with the North Atlantic Oscillation. *Clim. Change*, 36:301–326.

Jerlov, N. J. (1968). Optical oceanography. Elsevier.

Kimoto, M., Ghil, M., and Mo, K. C. (1991). Spatial structure of the extratropical 40-day oscillation. In *Proc. 8th Conf.Atmos.Oceanic Waves and Stability.*, pages 115–116. Amer.Meteor.Soc., Boston.

Kuo, H. L. (1964). On the formation and intensification of tropical cyclones through latent heat release by cumulus convection. *J. Atmos. Sci.*, 21:40–63.

Kushnir, Y. (1994). Interdecadal variations in North Atlantic sea surface temperature and associated atmospheric conditions. *J. Climate.*, 7:141–157.

Latif, M. and Barnett, T. P. (1994). Causes of decadal climate variability over the North Pacific and North America. *Science*, 266:634–637.

Le Treut, H. and Li, Z. X. (1991). Sensitivity of an Atmospheric General Circulation Model to prescribed SST changes: feedback effects associated with the simulation of cloud optical properties. *Climate Dyn.*, 5:175–187.

Madec, G. and Imbard, M. (1996). A global ocean mesh to overcome the North Pole singularity. *Climate Dyn.*, 12:381–388.

Manabe, S. and Strickler, R. F. (1964). On the thermal equilibrium of the atmosphere with convective adjustment. *J. Atmos. Sci.*, 21:361–385.

Morcrette, J. J. (1990). Impact of changes to the radiation transfer parameterizations plus cloud optical properties in the ECMWF model. *Mon. Weather. Rev.*, 118:847–873.

Moron, V., Vautard, R., and Ghil, M. (1996). Trends, interdecadal and interannual oscillations in global sea-surface temperatures. *Submitted to Climate Dyn.*

Paulson, C. A. and Simpson, J. J. (1977). Irradiance measurements in the upper ocean. *J. Phys. Oceanogr.*, 7:952–956.

Plaut, G. and Vautard, R. (1994). Spells of low-frequency oscillations and weather regimes in the northern hemisphere. *J. Atmos. Sci.*, 51(2):210–236.

Robertson, A. W., Ma, C. C., Mechoso, C. R., and Ghil, M. (1995). Simulation of the tropical Pacific climate with a Coupled Ocean-Atmosphere General Circulation Model. Part II: interannual variability. *J. Climate.*, 8:1199–1216.

Sadourny, R. (1975a). The dynamics of finite difference models of the shallow water equations. *J. Atmos. Sci.*, 32:680–689.

Sadourny, R. (1975b). Compressible model flows on the sphere. *J. Atmos. Sci.*, 32:2103–2110.

Sadourny, R. and Laval, K. (1984). January and July performance of the LMD general circulation model. In *New Perspectives in Climate Modelling*, pages 173–198. Elsevier Science Publishers, Amsterdam.

Selten, F. M., Haarsma, R. J., and Opsteegh, J. D. (1997). On the mechanism of North Atlantic decadal variability. *Submitted to J. Climate.*

Sutton, R. T. and Allen, M. R. (1997). Decadal predictability of North Atlantic sea surface temperature and climate. *Nature*, 388:563–567.

Terray, L. (1994). The OASIS coupled user guide version 1.0. Technical report, CERFACS TR/CMGC/94-33.

Unesco (1983). Algorithms for computation of fundamental property of sea water. Technical report, Unesco Techn Pap Mar Sci, 44.

Vautard, R., Yiou, P., and Ghil, M. (1992). Singular-spectrum analysis: A toolkit for short. noisy chaotic signals. *Physica D*, 58:95–126.

Vintzileos, A., Delecluse, P., and Sadourny, R. (1997). On the mechanisms in a Tropical Ocean-Global Atmosphere Circulation Model: Part II: interannual variability and its relation with the seasonal cycle. *Submitted to Climate Dyn.*

Weaver, A. J. and Sarachik, E. S. (1991). Evidence for decadal variability in an Ocean Circulation Model: an advective mechanism. *Atmosphere-Ocean*, 29:197–231.

Zorita, E., Kharin, V., and von Storch, H. (1992). The atmospheric circulation and sea surface temperature in the North Atlantic area in winter: their interaction and relevance for Iberian precipitation. *J. Climate.*, 5:1097–1108.